"This is the peer reviewed version of the following article: Fleishman, G.D. and Pevtsov, A.A.: 2018, "Electric Currents in the Solar Atmosphere", AGU Geophysics Monographs series, 235, "Electric Currents in Geospace and Beyond", Editors: Andreas Keiling, Octav Marghitu, Michael Wheatland, 45-67, which has been published in final form at DOI: 10.1002/9781119324522.ch3. This article may be used for non-commercial purposes in accordance with Wiley Terms and Conditions for Use of Self-Archived Versions."

ELECTRIC CURRENTS IN THE SOLAR ATMOSPHERE

Gregory D. Fleishman[1] and Alexei A. Pevtsov[2,3]

We review historical and modern studies pertinent to the measurements, modeling, and role of electric current in the solar atmosphere. We describe how the electric current density is computed from the vector magnetic field measurement at photospheric and chromospheric levels and how it is modeled, using Nonlinear Force-Free Field (NLFFF) extrapolations, in the solar corona. Next, the roles of electric currents in plasma dynamics and heating, energy release, and acceleration and transport of nonthermal particles are discussed. We then consider some interesting properties of electron and ion components forming electric current in a multi-component plasma, the effect of the electric current on the Alfvén wave properties, current neutralization and redistribution during solar flares. We discuss present theories about the origin of electric currents from subphotospheric and photospheric motions. We conclude that evaluation of electric currents in the solar atmosphere has reached a high level of maturity and that accounting for the electric current is highly important for solar physics.

1. INTRODUCTION

The Sun's volume can crudely be divided onto its interior and the outer atmosphere. The interior includes the inner core (IC), the radiative zone (RZ), and the convection zone (CZ). While the IC and RZ together comprise about 98% of the mass of the Sun, these layers do not have any electric currents with appreciable observable effect on the visible surface. The solar magnetic field observed on the Sun's visible surface and electric currents associated with it are likely created either in a thin transition layer between the RZ and the CZ, or in the bulk of the CZ via the flows of ionized plasma, whose collective action is referred to as a dynamo [*Charbonneau*, 2013]. Once the magnetic field reaches a certain threshold, it becomes buoyant, and rises through the CZ towards the outer layer of solar atmosphere, or corona [*Cheung and Isobe*, 2014; *Fan*, 2009]. The transition between the CZ and corona takes place over two thin layers called the photosphere (about 500 km in average thickness) and the chromosphere ($\approx$ 2500 km) bounded by a thin transition region (TR). It is in the photosphere and the chromosphere, where the magnetic field vector can be routinely "measured directly," from which the electric currents are inferred.

Practically all major solar features observed in the photosphere are associated with magnetic fields (see Figure 1). Dark sunspots (Figure 1a) correspond to areas of strong magnetic field (see white and black concentrations in Figure 1d). There, the magnetic field inhibits transport of energy via convection, which explains why these areas are darker than their surroundings. In contrast, in the chromosphere (Figure 1b) and corona (Figure 1c), areas around sunspots appear as bright features suggesting either enhanced energy transport (bright plages in the chromosphere) or enhanced heating in the corona [waves, reconnection etc., see, e.g., *Hansteen et al.*, 2015]. As active regions decay, their magnetic field spreads over larger areas and weakens. The evolving remnants of active regions form large-scale neutral lines, which may support accumulation of cool chromospheric material forming prominences or chromospheric filaments—prominences when seen against the disk [*Mackay et al.*, 2010; *Parenti*, 2014]. Solar flares and coronal mass ejections, the two major sources of the interplanetary disturbances associated with space weather, are related to groups of sunspots (active regions) and erupting filaments/prominences. Large areas of open, weak magnetic field can be readily recognized in the corona as coronal holes [*Cranmer*, 2009, see large dark feature in the lower (south) part of the solar disk in Figure 1c]. Coro-

[1]Physics Department, Center for Solar-Terrestrial Research, New Jersey Institute of Technology Newark, NJ, 07102-1982, USA.

[2]National Solar Observatory, Boulder, CO 80303, USA.

[3]ReSoLVE Centre of Excellence, Space Climate research unit, 90014 University of Oulu, Finland

Copyright 2017 by the American Geophysical Union.

nal holes are the areas from which the fast solar wind is launched.

Unlike laboratory measurements, any remote sensing of the electric current relies on measurements of the magnetic field vector and the use of Ampere's Law. Even though the determination of magnetic fields on the Sun refers to derivation of the magnetic field components from observations of various polarization states of spectral lines, we call such derivations "measurements," given that the results show a high level of repeatability and consistency when obtained by different observatories. It is true that the complexity in interpretation of the polarized light in terms of magnetic fields produces an uncertainty in the magnetic fields derived that way; however, those uncertainties can be firmly quantified. Similarly, "measurements" of electric currents refer to their computation from the given distribution of magnetic fields. The computation of electric currents involves spatial derivatives and so further increases the uncertainties associated with measurements of magnetic fields.

Currently available techniques of measuring magnetic field are based on the Zeeman and Hanle effects, and normally can only be applied to the photosphere and the chromosphere. Information about the polarity and the total field strength of the coronal magnetic field can be derived from the observations in radio wavelengths [for reviews, see *White*, 2005; *Gelfreikh*, 2004; *Gary et al.*, 2013; *Wang et al.*, 2015]. In some limited cases, information about the inclination of magnetic field vector relative to the line of sight can also be inferred [e.g., quasi-transverse propagation, QT-surface, *Ryabov et al.*, 2005]. The coronal field strength can also be derived via indirect measurements of oscillating coronal structures observed in EUV lines [e.g., *Nakariakov and Ofman*, 2001]. Direct measurements of the fields in low corona are possible via the Hanle effect in EUV resonance lines [*Raouafi*, 2002], or via the Zeeman effect in coronal spectral lines [*Harvey*, 1969; *Lin et al.*, 2000]. Since the corona is optically thin, the observed radiation represents an integral along the line-of-sight passing through multiple coronal structures. This complicates interpretation of magnetic fields measured this way. In contrast, the corona is optically thick in radio wavelengths, and thus, coronal fields obtained from radio methods are linked to specific layers in the solar corona, although there may be an uncertainty in the exact height of those layers. Traditionally, the derivation of coronal fields relied on their extrapolation from lower layers of the solar atmosphere. The extrapolation techniques make restrictive assumptions about the magnetic field as being either potential (vacuum or current-free) or force-free (linear or non-linear). The applicability of the force-free field approximation to solar atmospheric conditions depends on the ratio of gas (p) and magnetic pressures (commonly called the "plasma beta"): $\beta = \frac{8\pi p}{B^2}$. For $\beta \ll 1$, the pressure gradient can be neglected, and the stationary case of the equation of motion reduces to $\boldsymbol{j} \times \boldsymbol{B} = 0$, where $\boldsymbol{j}$ is the electric current density, and $\boldsymbol{B}$ is the

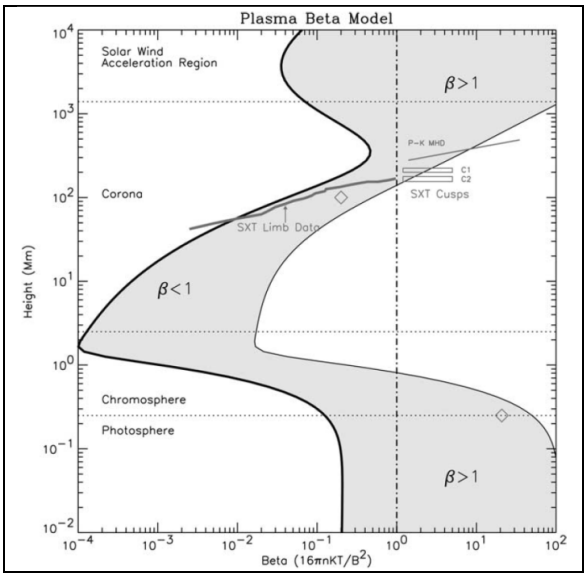

Figure 2. Compilation model of plasma β as a function of height in solar atmosphere above active region. Range of magnetic field is taken between (right boundary of shaded area) 150 G (representing plage) and 2500 G (sunspot, thick black line). From *Gary* [2001].

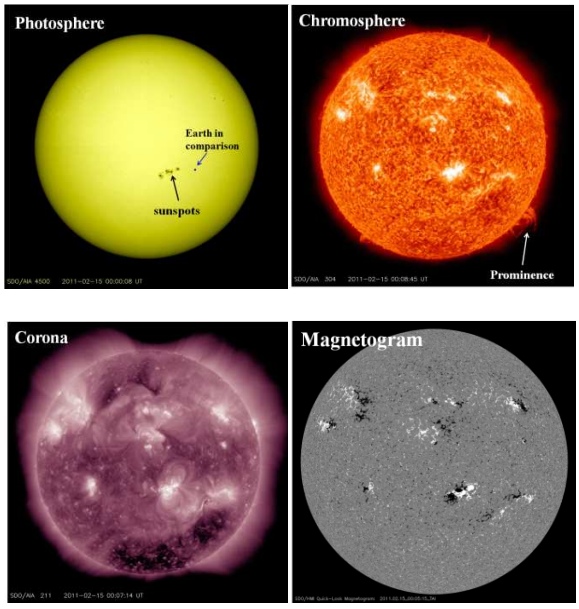

Figure 1. Images of the solar photosphere, chromosphere, and corona and the corresponding map of photospheric magnetic fields as observed by the Solar Dynamics Observatory on 15 Feb 2011 around 00:00 UT.

magnetic field. This "force-free field" (FFF) condition implies that the electric currents flow along the magnetic field.

The plasma properties differ significantly between the CZ, the photosphere, chromosphere, and corona. At its base (about 200,000 km below the photosphere), the CZ plasma is very dense ($\rho \simeq 0.1$ gm cm^{-3}) and is completely ionized ($T \simeq 2 \times 10^6$ K). The magnetic field strength is estimated to be in the range of a few dozens of kG. In the photosphere, $\rho \simeq 3 \times 10^{-7}$ gm cm^{-3} and $T \simeq 6,000$ K. The typical magnetic field strength in sunspots is about a few kilo-Gauss. This implies $\beta \gg 1$ through the convection zone and in the photosphere outside of strong field regions (e.g., sunspot umbrae). In the corona, the gas pressure and the magnetic field decrease significantly $\rho \simeq 10^{-16} - 10^{-14}$ gm cm^{-3}, $T = (1-2) \times 10^6$ K, and $B \simeq 10 - 100$ G (coronal holes/active regions). This results in $\beta \simeq 0.01 - 0.001 \ll 1$. A more detailed analysis (see Figure 2) indicates that the plasma β is smaller than unity in the range of heights from the mid-chromosphere to mid-upper corona. Evaluation of the plasma β based on observations of magnetic fields at different heights in the solar photosphere and the chromosphere suggests that the magnetic field is not force-free in the photosphere, while the FFF conditions are satisfied in the chromosphere [*Metcalf et al.*, 1995]. The reader should understand that these estimates of plasma β refer to average conditions. In various structures, the magnetic fields could be force-free or non-force-free even if these structures are located at the same height in solar atmosphere (see range of β in Figure 2).

Traditionally, the topological properties and interconnectivity of solar features in the photosphere and corona are presented in terms of their magnetic fields. For example, as a rule the sunspots are organized in groups, whose leading polarity is opposite in sign to the following polarity. The large-scale structure of magnetic field in bipolar active regions resembles the dipole field from a bar magnet. The polarity of leading spots in the Northern hemisphere is opposite to that in the Southern hemisphere [the so-called Hale or Hale-Nicholson polarity rule, *Hale and Nicholson*, 1925]. For the same group, the leading polarity spots are normally situated closer to the equator. The tilt of the main axis of a group relative to the equator varies approximately as sine of the latitude; this functional dependency is referred to as Joy's law. The Hale polarity rule is quite strong: only about 1-10% of active regions exhibit abnormal polarity orientation. But Joy's law is rather a weaker tendency with a significant scatter [for review, see, *Pevtsov et al.*, 2014].

Solar activity rises and falls with approximately 10-11 year cycles [*Hathaway*, 2010], although cycle-like variations with other periods were reported as well. At the beginning of a sunspot cycle, sunspots emerge at higher latitudes (normally, at about 40-45 degrees), and as the cycle progresses, the latitude of sunspot emergence moves slowly towards the equator. The leading polarity of sunspots reverses with each new cycle, and thus, the true magnetic cycle consists of two regular sunspot cycles. The solar cycle variation also includes polar magnetic fields. Polar fields have opposite polarity at the North and South polar caps. The maximum of the polar field is typically reached around the minimum of the sunspot cycle, and the two polar caps reverse their polarities shortly after the maximum of the sunspot cycle. Thus, during the rising phase of a sunspot cycle, the trailing polarity of sunspots in groups is opposite in sign to the polarity of polar magnetic field in the same hemisphere. During the declining phase of a sunspot cycle, the trailing polarity of sunspots in groups has the same sign as the polar field. This polarity orientation plays an important role in the solar cycle. As active regions (sunspot groups) decay, the magnetic flux of their following polarity is transported by the meridional flows to high latitudes. There it interacts with the existing polar field: first, canceling out the polar field of the previous cycle and later, rebuilding a new polar field of opposite sign for the next solar cycle. This qualitative representation of the evolution of solar magnetic field forms a foundation for the Babcock-Leighton dynamo model [*Babcock*, 1961].

The traditional "pictures" of solar phenomena are often based on magnetic field representations. Here we specifically refer to general descriptive picture, not MHD models. While the models (even at the dawn of the solar magnetography era) were based on equations that (directly or indirectly) include the electric currents, the descriptive pictures often shaped the interpretation of observations in the framework of these models. Thus, for example, for a long time, the observations did not consider electric currents developing as the result of reconnection, simply because at that time only magnetic field evolution was emphasized by qualitative pictures of this solar phenomenon. Perhaps, responding to that, *Alfvén and Carlqvist* [1967] had noted that a description based on electric currents is "often physically more interesting than a description in terms of magnetic field." The explicit use of electric currents provides another perspective allowing a deeper understanding the physics of generation (dynamo), topology (connectivity), restructuring (reconnection), and dissipation of solar magnetic

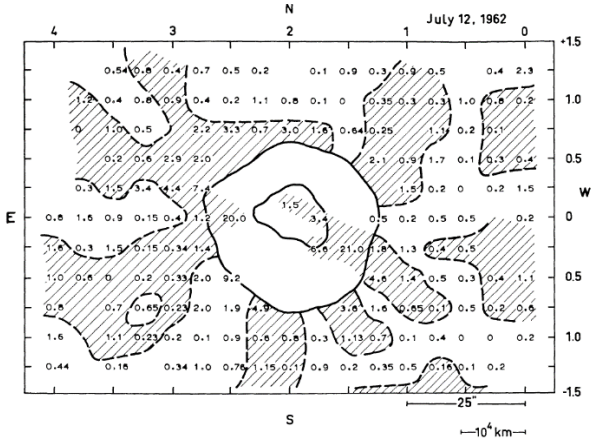

Figure 3. Map of vertical electric current density in a sunspot observed on July 12, 1962 at Crimean Astrophysical Observatory. Solid contours outline sunspot umbra and penumbra. X and Y axes indicate heliographic coordinates in degrees. Dashed lines mark boundaries between electric currents of negative (shaded) and positive sign. Note that electric currents of both sign are present in sunspot umbra and penumbra. This is a modified version of Figure 4 from *Severnyi* [1965].

fields. Thus, for example, the use of electric currents led to the introduction of the concept of magnetic and current helicity to solar physics in the 1990s [*Seehafer*, 1990; *Pevtsov et al.*, 1994; *Rust*, 1994; *Pevtsov et al.*, 1995; *Abramenko et al.*, 1996; *Zhang and Bao*, 1998]. As a quick reference, the helicity density is defined as a dot product of a vector and its curl; for example, the current helicity density is $h_c = \boldsymbol{B} \cdot [\nabla \times \boldsymbol{B}]$. The electric currents were shown to play a role in the reconnection process affecting both the reconnection itself [e.g., *Canfield et al.*, 1996], and the amount of energy released as the result of the reconnection [e.g., *Melrose*, 1997; *Kusano et al.*, 2004]. For more details on current/magnetic helicity and the role of electric currents in reconnection see reviews by *Brown et al.* [1999]; *Buechner and Pevtsov* [2003]; *Pevtsov et al.* [2014].

The earliest observations of electric currents in sunspots (Figure 3) were conducted in 1962 at Crimean Astrophysical Observatory [CrAO, see references to 1964 reports in *Severnyi*, 1965], and were based on differential form of Ampere's law: $\nabla \times \boldsymbol{B} = \frac{4\pi}{c}\boldsymbol{j} + \frac{1}{c}\frac{\partial \boldsymbol{D}}{\partial t}$ with the displacement term $\boldsymbol{D}$ neglected. Since the observations of vector field on the Sun are normally limited to a single height in the atmosphere, only the vertical (z) component of the electric current density could be derived as: $j_z = \frac{c}{4\pi}\left(\frac{\partial B_x}{\partial y} - \frac{\partial B_y}{\partial x}\right)$. Later, the photospheric electric currents in sunspots were also studied by *Moreton and Severny* [1968]; *Harvey* [1969]; *Rayrole and Semel* [1970].

In 1968, the first vector magnetograms at the chromospheric heights were observed in CrAO, and the electric currents in the photosphere and the chromosphere were found to be about the same [*Kotov*, 1970, 1972]. Observations taken in two photospheric lines forming at slightly different heights were used to compute horizontal components of electric currents. The horizontal electric currents were found to be larger than the vertical current [*Kotov*, 1971]. *Dravins* [1974] confirmed early findings made by Crimean astronomers. The average current density is sunspots was found to be about 9×10^{-3} A m^{-2} and about 3×10^{-3} A m^{-2} outside the sunspot outer boundary. The vertical currents were smaller than the horizontal ones. Later, *Hofmann and Staude* [1987] estimated the azimuthal component of electric currents assuming a specific geometry of a highly inclined flux tube forming an isolated sunspot to be about $(78 \pm 36) \times 10^{-3}$ A m^{-2}. *Pevtsov and Peregud* [1990] assumed an azimuthal (cylindrical) symmetry to derive the three components of electric current. Both studies confirmed that the horizontal currents in sunspots are typically larger than the vertical currents.

Computation of electric currents based on the differential form of Ampère's equation may be a subject of several uncertainties. First, the 180-degree ambiguity in the horizontal field direction needs to be resolved. This ambiguity arises from the classical definition of the azimuth of the horizontal magnetic field as the arctangent of the ratio of the Stokes Q and U components. These Stokes components represent properties of the linear polarization of light (see Section 2). The methods employed for the disambiguation are based on additional assumptions about the properties of the magnetic field in the solar atmosphere [for review, see, *Metcalf et al.*, 2006]. Ambiguity-free determination of total electric current in solar active regions has been formulated by *Semel and Skumanich* [1998], but has not been widely adopted. Second, taking partial derivatives tends to amplify the observing errors. Typically, the errors in the horizontal fields are an order of magnitude larger than the errors in the line-of-sight component. Alternatively, one can rewrite the Ampère's equation in integral form as:

$$\oint_C \boldsymbol{B} \cdot d\boldsymbol{l} = \frac{4\pi}{c}\int \boldsymbol{j} \cdot d\boldsymbol{S} = \frac{4\pi}{c}\boldsymbol{J}. \qquad (1)$$

Integrating horizontal field over the closed contour encompassing a flux element would give the total electric current crossing the surface of this flux element. This approach was briefly discussed in *Rayrole and Semel* [1970], and later used by several researchers [e.g., see, *Gopasyuk*, 2015, and refer-

ences therein]. The total currents found by the two methods seem to agree reasonably well.

2. MODERN MEASUREMENTS OF ELECTRIC CURRENT AT THE PHOTOSPHERE

Modern measurements of electric currents in the solar atmosphere follow the early approaches using the differential form of Ampère's law. Measurements of the vector magnetic field, however, have made significant progress. In the early days, the observations were often limited to measuring an integrated polarization over a restricted wavelength range in a wing of spectral line sensitive to the magnetic field in the range of atmospheric heights where this line is formed. To convert these polarization measurements to magnetic field (field strength, inclination, and azimuth) required making additional restrictive assumptions about the solar atmosphere, assuming a functional dependence between the degree of polarization and the magnetic field strength and orientation, as well as simplified radiative transfer modeling. While magnetographs of that type (often referred to as a Babcock-type magnetograph) are still in use, the majority of modern instruments are full-Stokes polarimeters, which sample a full spectral range associated with a spectral line and the neighboring continuum with sufficiently high spectral resolution. Observations are taken to characterize all four Stokes parameters: the total intensity, I, the circularly polarized component, V, and the two linearly polarized components, Q and U. Q and U are defined in coordinate systems rotated by 45° relative to each other. For example, if $+Q$ is maximum at zero and 180° azimuthal orientations (where the reference direction is set by the orientation of the optical element in a magnetograph), and $-Q$ is maximum at 90° and 270°, for $+U$ ($-U$) the maxima will be at 45° and 225° (135° and 315°) accordingly. The observations of Stokes I, Q, U, and V profiles are inverted to derive a set of thermodynamic and magnetic field parameters best fitting the observed spectro-polarimetry data. This approach has fewer restrictive assumptions, and it mitigates the presence of magneto-optical effects in measurements [*del Toro Iniesta*, 2003]. It also allows determining the gradients of magnetic field with height within the range of formation of the spectral line, and the fractional contribution of polarized and non-polarized light within each observing pixel. The latter parameter, often referred to as fill-(or filling) factor, provides an estimate of unresolved features with the magnetic field inside a single instrument pixel. A fill-factor of unity corresponds to totally magnetized plasma within the observing pixel, while $f = 0$ means that there is no contribution of magnetic field in any portion of the observed pixel.

Radiative transfer calculations may still use some simplified models of solar atmosphere, although these restrictions have gradually been relaxed. One of the model atmospheres most frequently employed by many inversion techniques is the so-called Milne-Eddington (ME) model. This model makes several assumptions, including: Local Thermodynamic Equilibrium (LTE); no depth dependence of the ratio of the spectral line to the continuum; linearity of the Planck function with depth in the stellar atmosphere; and no gradients in the magnetic field and the line absorption matrix (absorption coefficient, line damping, Doppler width and velocity) in the spectral line formation region. Under these assumptions, one could derive an analytical solution of the radiative trans-

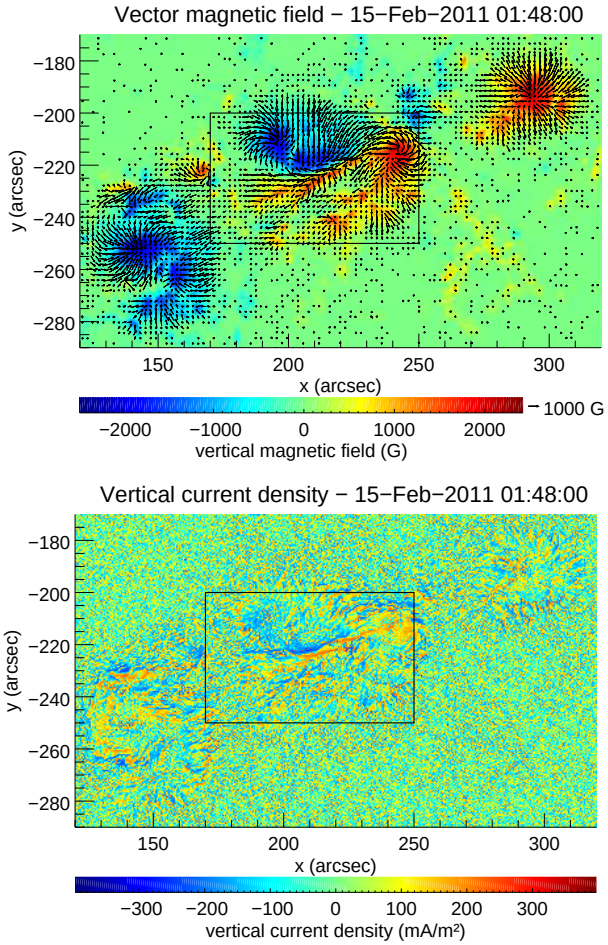

Figure 4. Maps of magnetic field (top) and j_z (bottom) derived from SDO/HMI observations of NOAA AR 11158 on February 15 2011. Note that electric currents of both sign are present in sunspot single polarity areas. The strongest currents are located along the magnetic neutral line separating two sunspots, which is also the area of strongest magnetic shear. From *Musset et al.* [2015], Figure 1.

fer equations, which was done by *Unno* [1956] and *Rachkovsky* [1962, 1967] in the early 1960s; for a recent review, see *del Toro Iniesta and Ruiz Cobo* [2016]. The inversion techniques that were developed later use this Unno-Rachkovsky analytical solution to fit the observed Stokes line profiles with the analytical ones with several (typically, six) free parameters.

Full-Stokes inversions based on the ME model are currently in use in such instruments as the Helioseismic and Magnetic Imager [HMI, *Scherrer et al.*, 2012; *Schou et al.*, 2012], the Vector StokesMagnetograph (VSM) at the Synoptic Optical Long-Term Investigations of the Sun facility [SOLIS, *Keller et al.*, 2003; *Balasubramaniam and Pevtsov*, 2011], the Imaging Magnetograph eXperiment (IMaX) for the Sunrise Balloon-Borne Solar Observatory [*Martínez Pillet et al.*, 2011], and the Spectropolarimeter (SP) on the Hinode spacecraft [*Kosugi et al.*, 2007]. For a more complete review of modern measurements of magnetic fields the reader is referred to *del Toro Iniesta* [2003].

2.1. Vertical Currents at the Photosphere

Figure 4 shows an example of the maps of the full vector magnetic field and vertical electric current density derived from the HMI/SDO observations. The distribution of electric currents in sunspots is highly structured. The strongest currents flow along the area of the strongest shear in the magnetic field (see the narrow elongated patterns of positive and negative currents inside the box shown in Figure 4). Currents flowing in umbral areas of sunspots are more disorganized, and both positive and negative currents are present inside each umbra (compare current distribution in darkest (blue or red) areas in Figure 4, top). As each sunspot is comprised of a single polarity magnetic field (positive or negative), the presence of oppositely directed currents indicates that the current helicity (h_c) of any single sunspot is sign-alternating. Such a pattern of current helicity is typical for most sunspots [*Gary et al.*, 1987; *Pevtsov and Peregud*, 1990; *Pevtsov et al.*, 1994], although highly twisted δ-spots often exhibit strong electric currents of a single sign inside each umbra [*Pevtsov*, 2005] with opposite currents flowing in opposite magnetic polarities. Individual patches of current helicity inside sunspot umbra have a lifetime of about 27 hours [*Pevtsov et al.*, 1994], which provides an estimate for a lifetime of isolated currents in sunspots in the absence of continuous generation or flare activity.

2.2. 3D Picture at the Photosphere

Because of a combination of the narrow height range of the photosphere ($\approx$ 500 km) and a simplified treatment of the radiative transfer (widespread use of Milne-Eddington stellar atmosphere), the 3D picture of electric currents in the photosphere is not well-studied.

High resolution observations of sunspots from instruments on Hinode spacecraft reveal highly structured patterns of electric currents in sunspot penumbra [*Gosain et al.*, 2014]. The pattern is well-correlated with the pattern of the penumbral filaments, and it suggests the presence of strong electric current flowing around these filaments. These electric currents are limited to the photosphere, and are unlikely to cross into higher layers of the solar atmosphere.

Puschmann et al. [2010a] applied the Stokes Inversion based on Response functions (SIR) algorithm to invert the Stokes profiles observed by Hinode/SP. The optical depth retrieved from SIR inversions was converted to geometric depth using the genetic algorithm developed by *Puschmann et al.* [2010b]. The algorithm finds a solution for the three components of a vector field by minimizing a merit function comprised of the weighted contributions of the magnetic field divergence and the residual force (which includes the pressure gradient, Lorentz force, and gravity). A 3D model of the magnetic field in a sunspot penumbra was constructed on the basis of geometric heights derived from this inversion. The magnetic field and electric currents at the photospheric heights of 200 km resulting from this inversion are shown in Figure 5 (left). The topology of the magnetic field in the sunspot penumbra was found to most closely correspond to the so-called uncombed model of sunspot penumbra, where nearly horizontal magnetic flux tubes (so-called intraspines) are embedded in stronger and more vertical magnetic field (so called spines). The pattern can be visualized by putting two hands together at a small angle and inserting fingers on one hand between the fingers on the other hand. In Figure 5, the locations of intraspines are outlined by white contours. Strong horizontal currents were found at the boundaries of intraspines. The direction of $\boldsymbol{j}_\perp$ at intraspine boundaries forms a slight (about 20 degrees) angle relative to the main axis of each horizontal flux tube (intraspine). The overall picture of these currents was interpreted as if they were flowing around a magnetic flux tube. At the low photospheric boundary (0 km), the plasma β in intraspines is larger than unity (corresponding to non-FFF conditions, Figure 5, right), while in spines and the photospheric upper boundary, $\beta \approx 0.1$. At the top layer of the photosphere, the magnetic field was found to satisfy a FFF condition; no significant currents were found in spines (the magnetic field was nearly potential there). Amplitudes of the horizontal current densities were about 3-4 times larger than those of the vertical ones, which agrees

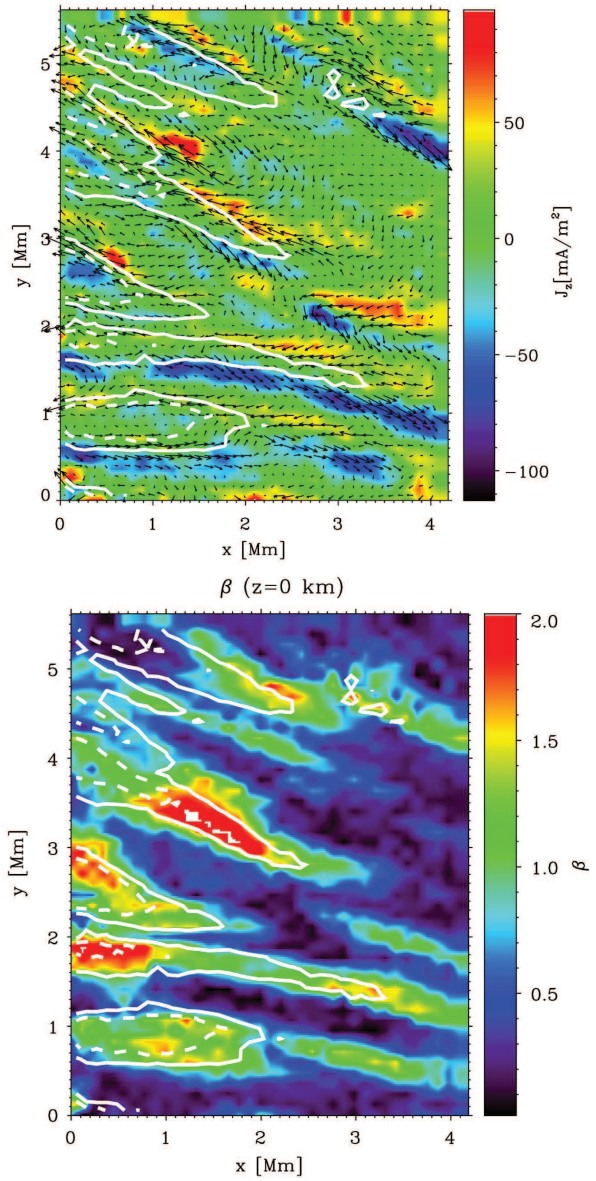

Figure 5. Top panel shows color-coded j_z and arrow-size-coded $\boldsymbol{j}_\perp$ at $z = 200$ km. Bottom panel shows a map of plasma β at $z = 0$ km. In both panels, white contours correspond to $B_z = -650$ G (solid lines) and $B_z = -450$ G (dashed lines) outlining intraspines. This is a modified version of Figures 1 and 4 from *Puschmann et al.* [2010a] © AAS. Reproduced with permission.

with previous derivations of electric currents [*Kotov*, 1971; *Hofmann and Staude*, 1987; *Pevtsov and Peregud*, 1990]. The peak amplitude of horizontal currents was $\gtrsim 120$ mA m^{-2}, which also agrees with some early derivations.

The authors also evaluated the amplitude of electric current using a more traditional approach based on inversion of magnetic fields in the framework of the ME atmosphere. This derivation showed that traditional inversions tend to significantly underestimate the total electric current. *Gosain et al.* [2014] also noted that ignoring the

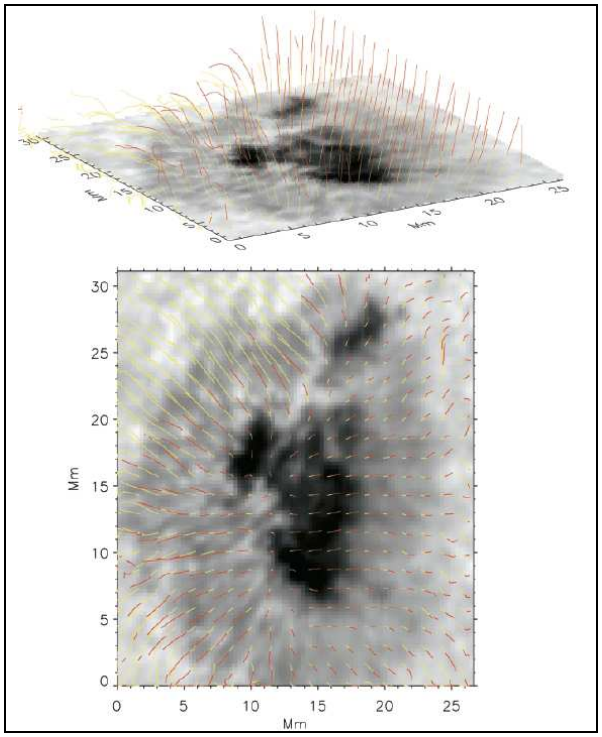

Figure 6. Visualization of the 3D magnetic structure above a sunspot in the perspective view (top panel) and top view (bottom panel). The bottom part (0–800 km) of the field lines is shown yellow, the top part (800–1600 km) is shown red. From *Socas-Navarro* [2005a] © AAS. Reproduced with permission.

fact that the optical depth varies slightly between spines and intraspines (and instead, assigning all observed fields to the same height in atmosphere) may lead to the appearance of false currents on top of the real ones.

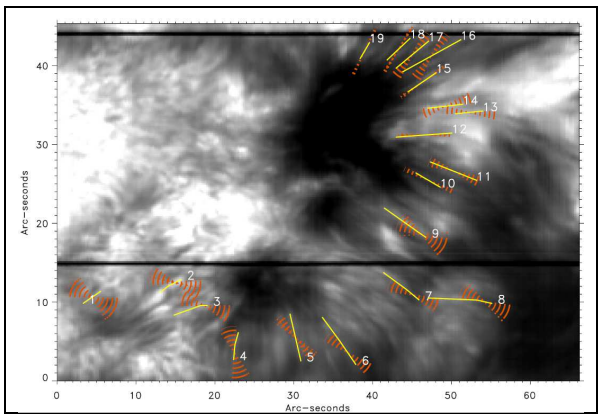

Figure 7. Example of misalignment between Hα fibrils (shown as yellow segments) and ranges of the azimuth of the magnetic field vector (red cones that take errors into account). From *de la Cruz Rodríguez and Socas-Navarro* [2011].

3. MEASUREMENTS OF ELECTRIC CURRENT AT THE CHROMOSPHERE

Measurement of the magnetic field vector in the chromosphere is a much more challenging task than in the photosphere. The chromosphere cannot be represented well by a uniform spherical layer, which complicates the interpretation of observations greatly; the chromospheric processes are rapid and often small-scale, thus requiring rapid measurements. At the same time, the magnetic field becomes on average weaker. Available measurements employ the few infrared magnetically sensitive lines, whose formation heights are located at the chromospheric levels such as He I 1083.0 nm or Ca II 854.2 nm. In addition to being more challenging observationally, the inversion of these chromospheric measurements is also challenging both theoretically and computationally. Indeed, there is no simple model of the chromosphere, such as the ME photospheric model, and thus there is no simple analytical solution of the radiative transfer equation to be fit to the data. The radiative transfer through the chromosphere is complicated by deviation from LTE and the presence of strong vertical gradients in the involved parameters. Accurate inclusion of all physical processes relevant to the inversion algorithm makes it computationally expensive. But an account of the realistic atmospheric conditions is needed for reliable vector magnetometry [*Lites et al.*, 1994; *Socas-Navarro*, 2002] because the outcome of the radiative transfer depends strongly on the atmospheric conditions.

Here we review some results on the chromospheric vector magnetometry and on the electric currents derived from the magnetic vector data following papers by *Socas-Navarro* [2005a] and *de la Cruz Rodríguez and Socas-Navarro* [2011]. *Socas-Navarro* [2005a] observed an active region (NOAA AR 0634) at the Sun using the Spectro-Polarimeter for Infrared and Optical Regions (SPINOR) instrument simultaneously in two photospheric Iron lines (849.7 and 853.8 nm) and two chromospheric Calcium lines (849.8 and 854.2 nm) to derive the magnetic field vector in a finite volume extending from the photospheric level up to high chromospheric heights.

The outcome of this analysis was a 3D distribution of the magnetic field vector above a sunspot, Figure 6. For convenience the lower portion (0–800 km) of the field lines is shown yellow, while the upper part (800–1600 km) is shown red. Importantly, the upper and lower parts behave consistently with each other: the divergence of the magnetic field is always small (less than 2%) compared with ratio of the magnetic field magnitude B and the box length l, B/l, which validates the 3D vector magnetic field reconstructed from the observations.

3.1. Misalignment Between Vectors of Magnetic Field and Hα Fibrils

Chromospheric fibrils are often considered to be tracers of horizontal magnetic field. Given that the plasma beta is small in the chromosphere, the magnetic configuration is supposed to be not far from a FFF configuration; thus, the electric current vector should be co-aligned with the chromospheric fibrils as well. This expectation was, in particular, employed by *Wiegelmann et al.* [2008] to fix the azimuth of the magnetic field at the chromospheric heights while performing Nonlinear FFF (NLFFF) extrapolation. *de la Cruz Rodríguez and Socas-Navarro* [2011] challenged this expectation. They tracked a number of Hα fibrils (shown as yellow line segments in Fig. 6 and compared them with the magnetic field azimuth shown by red cones, where the cone angle characterizes the uncertainty of the azimuth. It is apparent from the figure that Hα fibrils do not generally align with the magnetic field; thus, the use of the Hα fibrils as tracers of the magnetic field azimuth is not justified in the general case. There are a number of possible interpretations for this misalignment, of which the most plausible is, perhaps, the effect of ambipolar diffusion in the partly ionized plasma of the chromosphere [*Martínez-Sykora et al.*, 2016]. The point is that ions and neutrals will decouple as soon as the ion-neutral collision frequency is small. This means that the magnetic field is also decoupled from the neutral population and allows the field to slip through it.

3.2. Misalignment Between Vectors of Magnetic Field and Electric Current

Having the three-dimensional structure of the vector magnetic field, one can compute the vec-

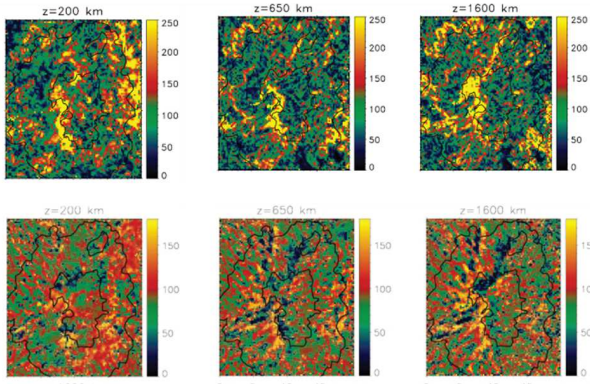

Figure 8. Distributions of the current density at different heights $z = 200, 650, 1600$ km (top); the scale is in mA m^{-2} for the sunspot shown in Figure 6. The angles between $\boldsymbol{j}$ and $\boldsymbol{B}$ are given in degrees. From *Socas-Navarro* [2005b] © AAS. Reproduced with permission.

tor current density as the curl of the field. *Socas-Navarro* [2005b] used SPINOR data described in the beginning of this section to compute the electric current vector in a finite volume above the sunspot; the results are summarized in Figure 8. The top row of this figure shows that the largest currents form filamentary structures, which look like 2D cuts of a current sheet system in 3D.

The low panels in Figure 8 show a systematic mis-alignment between the electric current and the magnetic field vectors. For a truly FFF, the angle between these two vectors should be either 0 or 180 degrees, and thus, the corresponding plots would be a combination of yellow and blue areas, which is clearly not the case. Instead, the bottom panels show considerable misalignment of the electric current vector from the magnetic field vector at all levels. This is indicative of a significant departure of the magnetic field from the force-free configuration even at a relatively high chromospheric level, although the departure is clearly weaker at the chromosphere compared with the photosphere: there are significant areas at the (inner part of the) chromospheric heights, where the field is close to force-free and the vectors are aligned well.

3.3. Role of Electric Current in Heating the Chromosphere

In addition to the magnetic field, modern inversions of Stokes profiles allow deriving several thermodynamic parameters of plasma, including its temperature. Figure 9 shows the distribution

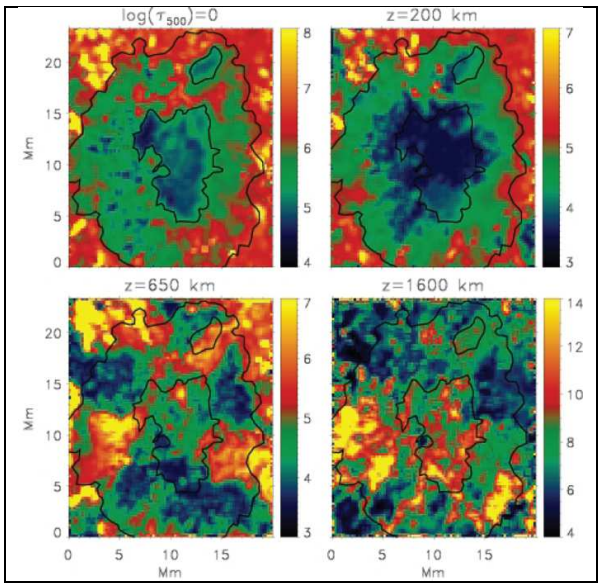

Figure 9. Temperature above the sunspot shown in Figure 6 derived from the inversion at various heights in the photosphere (0 and 200 km) and chromosphere (650 and 1600 km). Hot patches (≈ 5 Mm) embedded in a cooler plasma are seen at the chromospheric cuts. From *Socas-Navarro* [2005b] © AAS. Reproduced with permission.

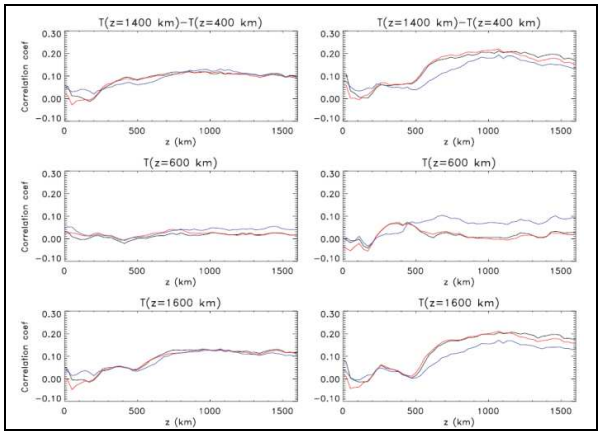

Figure 10. Correlation coefficients between temperature at a given height (labeled on top of the panel) and electric current density at the height z. Left: for the full area; right: for the penumbra only. Absolute value of the current is shown black, the perpendicular/red, and parallel/blue. From *Socas-Navarro* [2005b] © AAS. Reproduced with permission.

of the plasma temperature at various heights obtained this way. Even visual comparison of the temperature distribution (Figure 9) and electric current density distribution (Figure 8) show that they are remarkably different with no clear relationship between areas with strong chromospheric currents and the hot patches. This is further quantified by Figure 10, which shows spatial correlation between plasma temperature and electric current at various heights. Two observations can be made based on the correlation plots: although (1) the correlation coefficient is small, (2) it is positive almost everywhere. This is interpreted by *Socas-Navarro* [2005b] as indication that the dissipation of electric currents may contribute to the chromospheric heating, but this cannot be a dominant contribution.

The right panels in Figure 10 show the same correlation but restricted to a penumbral area only. Here the correlation coefficient increases by a factor of two indicating that the electric current dissipation may be a more important heating mechanism in the penumbra. *Goodman* [2004] advocated that the dissipation of Pedersen electric currents (flowing perpendicular to the magnetic field) is highly efficient in heating the solar chromosphere. Although the correlation curves for the entire region (Figure 10, left) do not show a clear distinction between both components, those for the penumbra (Figure 10, right) do show a slightly better correlation with the Pedersen component of the electric current. Contrary to that, *Arber et al.* [2016] argued that the heating provided by the dissipation of high-frequency Alfvén waves through Pedersen resistivity may be insufficient to balance the radia-

tive and conductive losses for a realistic range of field strengths and velocities.

The findings that the electric currents may play only a minor role in chromospheric heating are in qualitative agreement with *Fisher et al.* [1998], who studied a correlation between the total soft X-ray (SXR) brightness of active regions in the corona with several integral parameters and concluded that the magnetic flux is the prime component in this correlation. Once the correlation associated with magnetic flux is subtracted, the residual SXR brightness shows no correlation with the total electric current flowing in an active region.

4. MODELING OF ELECTRIC CURRENTS IN THE CORONA

There are a number of coronal magnetic field diagnostics [e.g., *Gibson et al.*, 2016; *Dalmasse et al.*, 2016] including radio methods, which provide either the absolute value of the magnetic field in the case of a gyroresonant process or the line-of-sight (LOS) component in the case of a polarized free-free process during non-flaring periods [e.g., *Lee*, 2007; *Wang et al.*, 2015] or the absolute value and the inclination of the magnetic field vector to the LOS in the case of the gyrosynchrotron process during flares [e.g., *Gary et al.*, 2013]. Only in rare cases are the magnetic field vector diagnostics available for dense, cool structures (e.g., prominences) located at coronal heights [*Orozco Suárez et al.*, 2014; *Levens et al.*, 2016]. The routine observational diagnostics to derive the magnetic field vector in the hot, tenuous corona are still in their infancy. Measurements of the three components of the vector field in the corona off the solar limb based on the Hanle effect are now taken with the the Coronal Multichannel Polarimeter [CoMP, *Tomczyk et al.*, 2008]. The observations represent a LOS column integration which may be difficult to interpret in terms of the physical 3D structure of the magnetic field. There are recent attempts to disentangle the LOS integration effect using coronal tomography [*Kramar et al.*, 2016].

In the current absence of routine observations, information on the magnetic field *vector* and electric current vector in the corona is derived from static (NLFFF), evolutionary (magnetofrictional), or dynamic (MHD) modeling augmented by one or another coronal diagnostics in some cases [*Wiegelmann and Sakurai*, 2012; *Wiegelmann et al.*, 2014]. Although the electric current, which plays an important role in the corona, is explicitly taken into account in both static NLFFF extrapolations and dynamic MHD models [see, e.g., recent reviews *Fan*, 2009; *Cheung and Isobe*, 2014; *Schmieder et al.*, 2014; *Chen*, 2011; *Shibata and Magara*, 2011; *Raouafi et al.*, 2016], often its role is not carefully considered or is even fully neglected, when interpreting observations.

4.1. Nonlinear Force-Free Field Extrapolations

Figure 2 shows that the plasma beta in the corona is less or much less than one; thus, there is no force available to balance the Lorentz force $\boldsymbol{j}\times\boldsymbol{B}$ [see, e.g., textbook by *Fleishman and Toptygin*, 2013a]. Therefore, a configuration with a significant Lorentz force must evolve towards a new configuration with a much smaller or no Lorentz force, which is called a FFF magnetic configuration. In particular, to have a stationary magneto-thermal configuration requires a magnetic field that is reasonably close to the FFF one.

Zero Lorentz force for a nonzero magnetic field and current density implies the electric current density vector directed along the magnetic field vector, $\boldsymbol{j}||\boldsymbol{B}$. Recalling that $\boldsymbol{j}\propto\nabla\times\boldsymbol{B}$ we conclude $\nabla\times\boldsymbol{B}=\alpha_{\rm FFF}\boldsymbol{B}$, where $\alpha_{\rm FFF}$ is a pseudo-scalar, called the FFF parameter. With the above relationships, we can write down the equations specifying the force-free magnetic field:

$$\nabla\times\boldsymbol{B}=\alpha_{\rm FFF}\boldsymbol{B},\qquad \boldsymbol{B}\cdot\nabla\alpha_{\rm FFF}=0. \quad (2)$$

A remarkable property apparent from Equation (2) is that the FFF parameter does not change in the direction of the magnetic field vector; as a result, $\alpha_{\rm FFF}$ does not change along any given field line. This property, at least theoretically, allows computing the electric current density along a given field line if the electric current density is

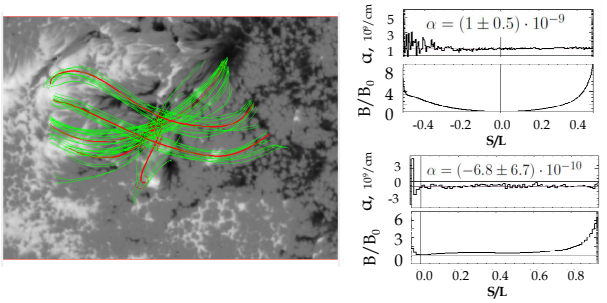

Figure 11. Visualization, using GX Simulator tool [*Nita et al.*, 2015], of a NLFFF data cube obtained with a Grad-Rubin method from *DeRosa et al.* [2015]. Grey image represents the bottom photospheric magnetogram, the red lines are the reference field lines, and the green lines are the flux tubes built around those reference field lines to visualize the magnetic field topology. Right panels show distributions of the $\alpha_{\rm FFF}$ parameter and the magnetic field modulus along two of the red field lines shown in the left panel.

known at the footpoint of this field line and the absolute value of the magnetic field is known along the field line, which requires less information about the magnetic field than for the use of Ampère's Law.

Vector magnetic field measurements at the photosphere and/or chromosphere represent a boundary from which the magnetic field in a coronal volume above this boundary can be reconstructed in the force-free regime [*Molodenskii*, 1969; *Aly*, 1984, 1989; *McClymont et al.*, 1997; *Schrijver et al.*, 2006; *Wiegelmann and Inhester*, 2010]. Theoretically, for some boundary conditions an FFF solution exists and it is unique [*Aly*, 1984; *Amari et al.*, 2006], although no solution may exist for an arbitrary boundary condition. Still, the uniqueness of NLFFF solution for given boundary conditions has been established only for small and smooth distributions of the force-free parameter alpha; and the actual meaning of smooth and small has yet to be determined [*Bineau*, 1972; *Boulmezaoud and Amari*, 2000]. Even when this problem has a unique solution, in practice a few reconstruction methods (called NLFFF extrapolations) including optimization [*Wheatland et al.*, 2000; *Wiegelmann et al.*, 2006; *Rudenko and Myshyakov*, 2009], magnetofrictional [e.g., *Valori et al.*, 2007], and Grad-Rubin [e.g., *Wheatland*, 2007] methods yield generally similar, but far from identical results [*De Rosa et al.*, 2009; *DeRosa et al.*, 2015]. In particular, the required constancy of the force-free parameter $\alpha_{\rm FFF}$ along a field line does not hold equally well in each of the methods; in particular, it does not hold well for various implementations of the optimization method. In contrast, the Grad-Rubin methods specifically attempt to preserve $\alpha_{\rm FFF}$ constancy along all closed field lines.

Figure 11 visualizes the 3D magnetic structure obtained with the Grad-Rubin method [*DeRosa et al.*, 2015] in a coronal volume above an AR with a number of reference field lines (red) and flux tubes (green) built around these reference field lines within a 3D modeling tool, GX Simulator [*Nita et al.*, 2015]. The panels to the right show how the force-free parameter $\alpha_{\rm FFF}$ and the absolute value of the magnetic field B vary along two of the red field lines. The plots show that the force-free parameter is reasonably constant along each of these two field lines; thus, the electric current density can straightforwardly be computed at any voxel as $\boldsymbol{j} = \frac{c}{4\pi}\alpha_{\rm FFF}\boldsymbol{B}$, where c is speed of light; thus the value of the electric current density drops along the field line proportionally to the magnetic field value. In the plotted field lines the footpoint-to-loop-top magnetic field ratio is about 5–8, thus, the electric current density at the loop top is, respectively, 5–8 times lower than at the corresponding foot point. This tells us that the strongest coronal currents must concentrate at the base of the corona, where the photospheric/chromospheric currents are strong and where the field lines show a reasonably small expansion.

4.2. Coronal MHD Modeling

No evolution of electric currents in the corona is captured by static NLFFF extrapolations; thus, modeling of the evolution requires explicit use of the time-dependent MHD approach, or possibly the magnetofrictional approach [*Cheung and DeRosa*, 2012; *Fisher et al.*, 2015]. The complete set of MHD equations that would be valid all the way from the (sub-) photospheric up to coronal heights is extremely complicated and expensive to solve numerically. Although advanced codes that take into account realistic physics exist [e.g., *Gudiksen et al.*, 2011], they can only be applied to a very limited spatial domain [*Carlsson et al.*, 2016]. In many cases, when only a coronal domain is studied, the modelers use a simplified set of MHD equations [e.g., *Jiang et al.*, 2016], which explicitly takes into account the condition of low-beta plasma $\beta \ll 1$. In this way, evolution of the magnetic field driven by photospheric motions results in progressively stronger tangling of the magnetic field lines due to freezing of the magnetic flux into the conductive fluid. Thus, the magnetic flux tubes become more strongly twisted, which implies enhancements of the corresponding electric current density along the flux tubes.

Here we briefly describe one example [*Amari et al.*, 2015] of a dynamic model driven by a "flux rope emergence" from the bottom of the modeling data cube. A magnetic structure was injected from the bottom with a significant twist and shear, and then was driven by the bottom (photospheric) velocity field. As a result, strong electric currents flowed in the volume, primarily along the magnetic field in the area of the flux rope emergence, which can be vividly seen from on-line movies that supplement the paper by *Amari et al.* [2015].

5. ELECTRIC CURRENT IN A HOT, MULTI-COMPONENT PLASMA

An interesting and nontrivial question is: What is the microscopic composition of electric currents in the hot corona, where atoms are ionized up to various ionization states, while there is no neutral component? It is clear that the electric current is primarily supported by a corresponding bulk motion of electrons, which are light and, thus, easier to accelerate given an electric force. It is also transparent that for a purely hydrogen fully ionized plasma, the protons will move along the electric field vector[1] (i.e., oppositely to the electrons)

with a bulk velocity consistent with momentum conservation. In the plasma rest frame we, thus, have $\boldsymbol{v}_p = -(m_e/m_p)\boldsymbol{v}_e \approx 5\times10^{-4}\boldsymbol{v}_e$. Then, the electron velocity is found from the equation $\boldsymbol{j} = \sum_c e_c n_c \boldsymbol{v}_c$, where the summation is performed over all plasma components. In our case we have two components with the same number densities, opposite charges, and strongly different masses; thus: $\boldsymbol{j} = -en_e\boldsymbol{v}_e(1+m_e/m_p)$, where e is the elementary positive charge, while $\boldsymbol{j}$ can be determined for the given electric field from Ohm's law.

A more complicated picture arises when there are other ions with larger charges (Ze) because momentum conservation alone is insufficient to determine the velocities of the plasma species and explicit consideration of their collisions with each other is needed. It was first performed by *Gurevich* [1961], who demonstrated that "multiply charged" positive ions move, *together* with negative electrons, in the direction *opposite* to the protons. A simple explanation of this effect is as follows. A stationary electric current is set up due to balancing the electric force ($\boldsymbol{F} = eZ\boldsymbol{E}$) by the dynamic friction forces (proportional to Z^2) between all plasma species. These two forces almost compensate each other in the case of protons ($Z = 1$), which results in a very small bulk velocity of the protons. But this implies that for any $Z > 1$, the dynamic drag force acting on the multiply charged ions by the fast moving electrons will overcome the net electric force; thus, the multiply charged ions will move in the same direction as the electrons. Quantitative consideration of this effect can be found in *Fleishman and Toptygin* [2013a, Section 11.1.1 and Figure 11.1 there], from where we estimate the bulk velocity of the protons and ions of abundant ^{4}He and much rarer ^{3}He ions for the typical solar abundances:

$$\boldsymbol{v}_p = -\frac{2n_4}{n_p+4n_4}\sqrt{\frac{m_e}{m_p}}\boldsymbol{v}_e \approx 2.9\times10^{-3}\boldsymbol{v}_e,$$

$$\boldsymbol{v}_4 = \frac{n_p}{2(n_p+4n_4)}\sqrt{\frac{m_e}{m_p}}\boldsymbol{v}_e \approx 8.8\times10^{-3}\boldsymbol{v}_e, \quad (3)$$

$$\boldsymbol{v}_3 = \frac{n_p n_4}{n_e(n_p+4n_4)}\boldsymbol{v}_e \approx 5\times10^{-2}\boldsymbol{v}_e.$$

From here we can draw a few important conclusions about components of the electric current in a multi-component plasma.

1. Protons move much faster than in a purely hydrogen plasma.

2. Helium ions move at the *same* direction as *electrons*, and oppositely to *protons*.

3. ^{3}He ions (and other rare ions) move much faster than ^{4}He ions (and other abundant ions).

This phenomenon is likely relevant for understanding enrichment of solar energetic particles by rare elements, most notably, ^{3}He, and also for variations of elemental abundances in the corona, reported recently for both flare [*Warren*, 2014] and active region [*Caspi et al.*, 2015] measurements.

6. ALFVÉN WAVE ON TOP OF CURRENT-CARRYING MAGNETIC FIELD

Another interesting effect of the electric current present in the plasma is a modification of plasma eigenmodes compared with the current-free case. A fundamental reason behind this modification is the breaking of the plasma's mirror symmetry, which can be quantified by a pseudoscalar quantity—nonzero current helicity density $h_c = \boldsymbol{B}\cdot[\nabla\times\boldsymbol{B}] \neq 0$. Here, for simplicity, we consider the corresponding current-induced modification to the Alfvén waves only. To do so, in the full set of MHD equations we neglect all dissipative terms as well as the pressure gradient and any external force, rather than the Lorentz force. The truncated set of equations reads:

$$\nabla\cdot\boldsymbol{B} = 0, \qquad \frac{\partial\boldsymbol{B}}{\partial t} = \nabla\times[\boldsymbol{u}\times\boldsymbol{B}], \quad (4a)$$

$$\rho\left(\frac{\partial\boldsymbol{u}}{\partial t} + (\boldsymbol{u}\cdot\nabla)\boldsymbol{u}\right) = \frac{1}{4\pi}[\nabla\times\boldsymbol{B}]\times\boldsymbol{B}. \quad (4b)$$

To determine the eigen mode, we have to linearize these equations assuming $\boldsymbol{B} = \boldsymbol{B}_0(\boldsymbol{r}) + \boldsymbol{b}$:

$$\frac{\partial\boldsymbol{b}}{\partial t} = (\boldsymbol{B}_0\cdot\nabla)\boldsymbol{u} - (\boldsymbol{u}\cdot\nabla)\boldsymbol{B}_0, \quad (5a)$$

$$\frac{\partial\boldsymbol{u}}{\partial t} = \frac{1}{4\pi\rho}(\nabla\times\boldsymbol{b})\times\boldsymbol{B}_0 + \frac{\alpha_{\rm FFF}}{4\pi\rho}\boldsymbol{B}_0\times\boldsymbol{b}, \quad (5b)$$

where $\boldsymbol{b}$ and $\boldsymbol{u}$ are the first-order oscillating values. In contrast to the classical case of the uniform mean magnetic field, in our case we have to take into account that $\nabla\times\boldsymbol{B}(\boldsymbol{r}) \neq 0$; thus, the linearized equations have additional terms (the last terms in each row; in the second one we assume that the field is force free and use $\nabla\times\boldsymbol{B}_0(\boldsymbol{r}) = \alpha_{\rm FFF}\boldsymbol{B}_0$) compared with the classical case. Accordingly, the solution describing properties of the Alfvén waves will also be different from the classical case. A remarkable modification of the Alfvén wave compared with the current-free case [see problem 2.6 in *Fleishman and Toptygin*, 2013a] is that the vectors $\boldsymbol{u}$ and $\boldsymbol{b}$ are not parallel to each other any longer, which has a number of important implications. In particular, the modified wave possesses a nonzero kinetic helicity [problem 2.6 in *Fleishman and Toptygin*, 2013a] $\langle h_k\rangle = \frac{1}{2}\Re\langle\boldsymbol{u}\cdot(\nabla\times\boldsymbol{u}^*)\rangle$, which is proportional to the force-free field parameter $\alpha_{\rm FFF}$.

Then, given that the vectors $\boldsymbol{b}$ and $\boldsymbol{u}$ are not parallel to each other any longer, the mean electric field of the Alfvén wave, $\boldsymbol{E}_h \propto \langle \boldsymbol{u} \times \boldsymbol{b} \rangle$, turns out to be non-zero. It is easy to estimate from consideration of dimensions [see Section 11.2.2 in *Fleishman and Toptygin*, 2013a, for quantitatve analysis] that this electric field is proportional to both the mean magnetic field and the FFF parameter $\boldsymbol{E}_h \propto \alpha_{\rm FFF} \boldsymbol{B}_0$. Remarkably, the direction of this electric field does NOT depend on the $\boldsymbol{k}$-vector, but on the $\boldsymbol{B}$-vector only. An ensemble of such Alfvén waves with random phases will represent a "helical" Alfvénic turbulence with properties distinct from the "standard" Alfvénic turbulence. In particular, given that the mentioned mean electric field has the same direction for all present Alfvén waves independently on their wavevectors, the magnitude of this electric field will go up for stronger and stronger turbulence (more and more waves). This electric field can become sufficiently large to form runaway particle populations that can be further picked up by stochastic acceleration by the same wave ensemble.

7. ELECTRIC CURRENT AND SOLAR FLARES

Various forms of eruptive activity at the sun are manifestations of excessive magnetic energy stored in the solar corona in a non-potential magnetic field, which is supported by electric currents. Solar flares, vividly seen as transient brightenings throughout electromagnetic spectrum from radio waves to gamma rays, represent the most rapid release of this excessive magnetic energy; thus, solar flares are closely linked with coronal electric currents. Given that the Reynolds number is overall large in the corona, the rapid energy release in flares requires that the currents are concentrated into small regions such as narrow current sheets. Non-flaring current sheets were inferred observationally [e.g., *Solanki et al.*, 2003] in the system of rising loops low in the corona at the regions with a tangential discontinuity of the field direction.

Within a standard model of solar flare, the energy release high in the corona results in acceleration of a fraction of plasma particles to nonthermal energies in an "acceleration region" (see Figure 12). Then, these particles precipitate down to the chromospheric footpoints, where they lose their energy in Coulomb collisions and produce X-ray and γ-ray emissions. Besides a variety of multifaceted manifestations, these precipitating particles represent a strong electric current, which would produce an additional magnetic field on top of the coronal one. Estimates with Ampère's law show that this magnetic field can be as large as $\approx 10^5$ G which would contain more energy than the beam itself. Prompt creation of such an intense magnetic field of $\sim 10^5$ G in the highly conductive corona would require either some type of anomalous resistivity to generate new flux or unrealistically rapid, coherent, and large-scale inflows to compress pre-existing flux. The commonly accepted solution for this paradox is creation of the neutralizing return current composed of background particles; see Figure 12.

7.1. Association Between X-ray Emission and Photospheric Currents

Although theoretically expected, detailed relationships between solar flares and electric currents in the solar atmosphere are not easy to establish observationally. *Janvier et al.* [2014] showed that the photospheric currents are concentrated in the

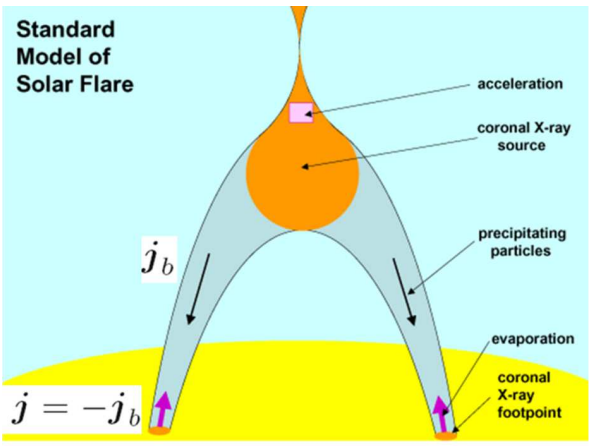

Figure 12. A cartoon showing a "standard" model of solar flare. Precipitating electrons form a 'direct' electric current $\boldsymbol{j}_b$, which is neutralized by a return current formed by background particles $\boldsymbol{j} = -\boldsymbol{j}_b$. A modified version of a figure from *Benz* [2008].

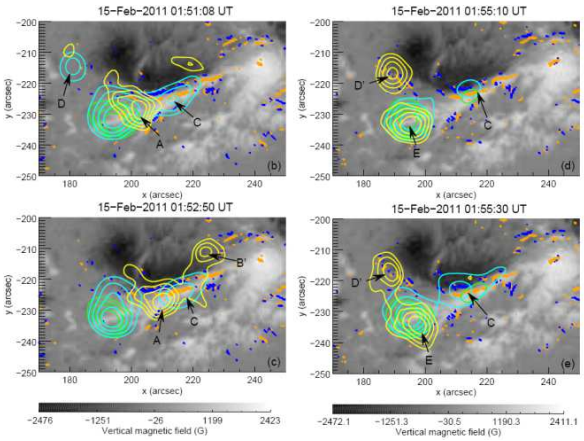

Figure 13. Association between photospheric magnetogram (gray image), photospheric positive (yellow dots) and negative (blue dots) currents, and X-ray emission in 12-25 keV (green contours), 25-50 keV (cyan contours), and 50-100 keV (yellow contours) energy ranges at different time frames for AR 11158 at the time of a solar flare (01:48:00 UT). From *Musset et al.* [2015].

"current ribbons," i.e., elongated areas or stripes of an enhanced current density. They presented evidence that the current ribbons, which are also correlated with the flare EUV ribbons, highlight the photospheric imprint of coronal electric current sheets. These current sheets may be formed where the gradient of magnetic connectivity is strong. Such areas are known to favor reconnection [see e.g. *Demoulin et al.*, 1996] that drives the solar flare. Thus, both electric currents and processes of plasma heating and particle acceleration in flares are expected to occur in these same regions. This suggests that the thermal and non-thermal X-ray emissions in solar flares are expected to be closely associated with the photospheric current ribbons.

Musset et al. [2015] reported on a close association between SXR observed with RHESSI and the photospheric electric current distribution derived from the SDO/HMI data, which is summarized in Figure 13. Although there is no "pixel-to-pixel" correlation between X-ray brightness and distribution of the electric current density, there are elongated thermal and non-thermal X-ray sources shown in green (12–25 keV) and cyan (25–50 keV) projected onto narrow elongated photospheric current ribbons. The high-energy source (50–100 keV) shown in yellow is supposed to trace the chromospheric footpoints of the flaring loops system. Thus, it is remarkable that the X-ray source A is projected onto the main current ribbon (black arrow in the top panel of Figure 13). The reported spatial relationships confirm the close association between locations of the acceleration region in this flare and electric current sheets.

7.2. Evolution of the Photospheric Current at the Course of Flare

It is interesting that in addition to the remarkable spatial relationships between hard X-ray (HXR) emission and photospheric currents, *Musset et al.* [2015] also found a coherent behavior of them in time. Specifically, the appearance of the 50-100 keV X-ray source D′ (upper right panel in Figure 13) is accompanied by simultaneous appearance of cospatial photospheric currents. *Kazachenko et al.* [2015] reported a global change of the magnetic field at the same AR during this flare accompanied by a decrease of magnetic field twist, which implies a corresponding reconfiguration of the electric current system at the course of the flare. It is worthwhile to note that the polarization measurements, on which the magnetic field data is based, can be biased during flares due to a number of known effects [see, e.g., *Hénoux and Karlický*, 2013, and references therein]. For this reason *Janvier et al.* [2014] and *Musset et al.* [2015] carefully analyzed the changes of the transverse magnetic field during the given flare and concluded that the derived changes of the vertical electric current are real.

This coherence in time evolution of the electric currents and HXR emission is strong evidence that magnetic reconnection is responsible for both these phenomena. Indeed, the observed rapid increase of the photospheric electric current density beneath the source D′ can be easily understood as a result of a reconnection between a flux tube carrying a strong current and another flux tube, perhaps, current-free or carrying a weaker current, which was initially rooted in the D′ area. After it reconnected with a current-carrying loop, the current will rapidly become uniform over the coronal portion of the newly formed flux system due to the requirement of the electric current continuity [e.g., *Canfield et al.*, 1996]. Thus, the photospheric electric current must go up at the corresponding footpoint, as observed. Another known outcome of magnetic reconnection is plasma heating and particle acceleration, which is traced by the HXR emission. We note that according to *Petrie* [2012] the relatively rapid changes in the electric current system reported by *Musset et al.* [2015] are not unique to the 2011-02-15 flare but likely typical for other flares as well.

8. ORIGIN OF ELECTRIC CURRENTS IN THE SOLAR ATMOSPHERE

Electric current observed in the upper solar atmosphere (photosphere and above) are believed to be either of subphotospheric origin or the result of stress applied to the magnetic field after its emergence. Early analysis of different mechanisms for supplying energy to solar flares suggested that while (near-) surface shear flows may contain sufficient energy for small flares, major flares and repeated flare activity require significant electric currents of sub-photospheric origin [*McClymont and Fisher*, 1989]. Observations do show that isolated bipolar flux elements emerge already carrying electric currents [e.g., *Leka et al.*, 1996] although the relative motions of footpoints of these flux tubes are also present as part of the flux emergence. The force balance at the interface of sub- and above-photospheric portions of a flux tube dictates a more complex dynamic behavior of the twist (and therefore, of the electric current). Temporal evolution of electric current in an emerging flux tube at the photospheric level will depend on the speed of emergence: if the emergence is relatively slow, the evolution of magnetic flux and electric current (twist) will follow each other, but for a rapid emergence, propagation of twist (electric current) will be delayed as compared with the magnetic flux [*Longcope and Welsch*, 2000]. Such predicted evolution of magnetic flux and twist (electric currents)

was observed in several small bipolar active regions [*Pevtsov et al.*, 2003]. The subphotospheric origin of electric currents is also supported by studies of the multifractality of the magnetic field of active regions [*Abramenko*, 2006] and comparative studies of the current helicity of photospheric and coronal magnetic fields [*Pevtsov et al.*, 1997]. *Gosain et al.* [2014] decomposed the observed vertical density of electric current (derived from high-resolution observations of vector magnetic field) into two components, parallel and orthogonal to the direction of the horizontal field. The second component was used to represent global electric current crossing from the photosphere to the chromosphere and corona. They found these global currents in agreement with the overall twist of the coronal structures above sunspots in support of idea of continuity of electric current flow between the photosphere and corona. The patterns of electric currents in δ-spots, where the umbra with one polarity field contains upward current and the umbra with the other polarity has downward current also supports the picture of electric current flowing from the photosphere in one footpoint of a flux tube, through the chromosphere, corona, and back to the photosphere in the other footpoint of the same flux tube [*Gopasyuk*, 2015; *Pevtsov*, 2005].

It has been argued that both mechanisms (subphotospheric origin and near-photosphere shear) can create neutralized currents: with main (direct) current flowing in the main body of a magnetic flux tube, and return current flowing in the opposite direction in a boundary layer of the tube [*Melrose*, 1991]. Studies based on low-moderate spatial resolution magnetograms consistently showed that electric currents in active regions are not neutralized in the photosphere. Summarizing findings of several studies, *Pevtsov et al.* [1997] concluded that the pattern and amplitude of j_z derived from vector magnetograms "cannot plausibly be explained on the basis of local currents that close in the photosphere." In a separate study of 21 active regions, *Wheatland* [2000] drew a similar conclusion that the large-scale electric currents flowing in solar active regions are usually unneutralized. References to additional studies addressing the question of observational aspects of neutralization of electric currents can be found in the citation lists of these two papers. Complementing these observations, numerical modeling also indicates that both the flux emergence and the photospheric flows acting on magnetic fields can build up unneutralized currents. Only in some rare circumstances i.e. when the photospheric neutral line does not have any magnetic shear, the action of the photospheric flows may result in completely neutralized currents. For a review of the numerical modeling of unneutralized electric currents the reader is referred to *Dalmasse et al.* [2015, and references therein].

The subphotospheric origin of electric currents lends support for the hypothesis that the emergence of active region magnetic fields carrying significant electric current can be used to predict the level of flaring activity of a given active region. In line with that hypothesis, *Bobra and Couvidat* [2015] reported that some of the strongest "photospheric" predictors of flare activity are related to electric currents.

9. CONCLUSIONS

A brief overview of observational and theoretical studies of electric currents in the solar atmosphere presented here demonstrates that the understanding and qualitative description of many solar processes from magnetic flux emergence[*Cheung and Isobe*, 2014; *Schmieder et al.*, 2014], to reconnection, flaring [*Raouafi et al.*, 2016], and particle acceleration [*Fleishman and Toptygin*, 2013b] may benefit tremendously from explicitly bringing electric currents into the picture. Although the assumption about a force-free field seems justifiable in the chromosphere on the basis of the low plasma β, observed mis-alignment between magnetic field and electric current vectors seems to contradict this. Observations also suggest that there may be electric current flowing outside and around magnetic flux bundles in sunspot penumbrae, and at the same time, the currents are continuous along the corresponding current circuit encompassing the photosphere, chromosphere, and corona. In interpretations of observations involving reconnection processes, the interaction of current-carrying magnetic structures and the re-distribution of electric currents need to be investigated [see, early work by *Canfield et al.*, 1996].

Finally, one might question if the electric currents derived from the limited spatial resolution magnetographic observations represent a fair approximation of the true electric currents flowing in the solar atmosphere. *Parker* [1996] showed that if a magnetic flux rope is comprised of isolated current-carrying magnetic filaments, the currents derived from magnetograph measurements that do not resolve individual threads would show no resemblance of the true currents flowing along the threads. However, we did not see any qualitative change in the overall picture of the electric currents in sunspots as the spatial resolution of magnetographic observations improved from about 1 arc second in 1960 to 0.1-0.15 arc seconds in mid-2010. The newer observations indicate the presence of return currents as predicted by the theory, and the data also support the continuity of electric

current from the photosphere, through the chromosphere and corona. Taken together, this justifies that modern magnetographic observations provide a physically correct representation of electric currents in the solar atmosphere. This picture is expected to be improved tremendously with a new generation of instruments including DKIST and FASR. Overall, we conclude that considering the electric current in addition to the magnetic field is essential to address many fundamental physical problems of solar physics.

ACKNOWLEDGMENTS. We are thankful to Dr. Michael Wheatland for critical reading of the manuscripts and his valuable comments. This work was supported in part by NSF grants AGS-1250374 and AGS-1262772, NASA grants NNX14AC87G and NNX16AL67G to New Jersey Institute of Technology and RFBR grant 15-02-03835. A.A.P. acknowledges the financial support by the Academy of Finland to the ReSoLVE Centre of Excellence (project no. 272157) and NASA grant NNX14AE05G.

NOTES

1. For simplicity, we adopt that electric field is elongated along the magnetic field, so no transverse or Hall current is considered, there is no $\boldsymbol{E} \times \boldsymbol{B}$ drift, etc.

REFERENCES

Abramenko, V. I. (2006), Emerging Active Regions: Turbulence in the Photosphere versus Flaring in the Corona, in *Solar MHD Theory and Observations: A High Spatial Resolution Perspective*, *Astronomical Society of the Pacific Conference Series*, vol. 354, edited by J. Leibacher, R. F. Stein, and H. Uitenbroek, p. 195.

Abramenko, V. I., T. Wang, and V. B. Yurchishin (1996), Analysis of Electric Current Helicity in Active Regions on the Basis of Vector Magnetograms, *Solar Phys.*, *168*, 75–89, doi:10.1007/BF00145826.

Alfvén, H., and P. Carlqvist (1967), Currents in the Solar Atmosphere and a Theory of Solar Flares, *Solar Phys.*, *1*, 220–228, doi:10.1007/BF00150857.

Aly, J. J. (1984), On some properties of force-free magnetic fields in infinite regions of space, *Astrophys. J.,* , *283*, 349–362, doi:10.1086/162313.

Aly, J. J. (1989), On the reconstruction of the nonlinear force-free coronal magnetic field from boundary data, *Solar Phys.*, *120*, 19–48, doi:10.1007/BF00148533.

Amari, T., T. Z. Boulmezaoud, and J. J. Aly (2006), Well posed reconstruction of the solar coronal magnetic field, *Astron. Astrophys.,* , *446*, 691–705, doi:10.1051/0004-6361:20054076.

Amari, T., J.-F. Luciani, and J.-J. Aly (2015), Small-scale dynamo magnetism as the driver for heating the solar atmosphere, *Nature*, *522*, 188–191, doi:10.1038/nature14478.

Arber, T. D., C. S. Brady, and S. Shelyag (2016), Alfvén Wave Heating of the Solar Chromosphere: 1.5D Models, *Astrophys. J.,* , *817*, 94, doi:10.3847/0004-637X/817/2/94.

Babcock, H. W. (1961), The Topology of the Sun's Magnetic Field and the 22-YEAR Cycle., *Astrophys. J.,* , *133*, 572, doi:10.1086/147060.

Balasubramaniam, K. S., and A. Pevtsov (2011), Ground-based synoptic instrumentation for solar observations, in *Solar Physics and Space Weather Instrumentation IV*, *Proc. SPIE*, vol. 8148, p. 814809, doi:10.1117/12.892824.

Benz, A. O. (2008), Flare Observations, *Living Reviews in Solar Physics*, *5*, 1, doi:10.12942/lrsp-2008-1.

Bineau, M. (1972), On the existence of force-free magnetic fields, *Communications on Pure and Applied Mathematics*, *25*(1), 77–84, doi:10.1002/cpa.3160250107.

Bobra, M. G., and S. Couvidat (2015), Solar Flare Prediction Using SDO/HMI Vector Magnetic Field Data with a Machine-learning Algorithm, *Astrophys. J.,* , *798*, 135, doi:10.1088/0004-637X/798/2/135.

Boulmezaoud, T. Z., and T. Amari (2000), On the existence of non-linear force-free fields in three-dimensional domains, *Zeitschrift Angewandte Mathematik und Physik*, *51*, 942–967.

Brown, M. R., R. C. Canfield, and A. A. Pevtsov (1999), *Magnetic Helicity in Space and Laboratory Plasmas*, vol. 111, American Geophysical Union, Washington D.C., doi:10.1029/GM111.

Buechner, J., and A. A. Pevtsov (2003), Preface, *Advances in Space Research*, *32*, 1817–1817, doi:10.1016/S0273-1177(03)90615-6.

Canfield, R. C., A. A. Pevtsov, and A. N. McClymont (1996), Magnetic chirality and coronal reconnection., in *Magnetic Reconnection in the Solar Atmosphere*, *Astronomical Society of the Pacific Conference Series*, vol. 111, edited by R. D. Bentley and J. T. Mariska, pp. 341–346.

Carlsson, M., V. H. Hansteen, B. V. Gudiksen, J. Leenaarts, and B. De Pontieu (2016), A publicly available simulation of an enhanced network region of the Sun, *Astron. Astrophys.,* , *585*, A4, doi:10.1051/0004-6361/201527226.

Caspi, A., T. N. Woods, and H. P. Warren (2015), New Observations of the Solar 0.5-5 keV Soft X-Ray Spectrum, *Astrophys. J.,* , *802*, L2, doi:10.1088/2041-8205/802/1/L2.

Charbonneau, P. (2013), Where is the solar dynamo?, *Journal of Physics Conference Series*, *440*(1), 012014, doi:10.1088/1742-6596/440/1/012014.

Chen, P. F. (2011), Coronal Mass Ejections: Models and Their Observational Basis, *Living Reviews in Solar Physics*, *8*, 1, doi:10.12942/lrsp-2011-1.

Cheung, M. C. M., and M. L. DeRosa (2012), A Method for Data-driven Simulations of Evolving Solar Active Regions, *Astrophys. J.,* , *757*, 147, doi:10.1088/0004-637X/757/2/147.

Cheung, M. C. M., and H. Isobe (2014), Flux Emergence (Theory), *Living Reviews in Solar Physics*, *11*, 3, doi:10.12942/lrsp-2014-3.

Cranmer, S. R. (2009), Coronal Holes, *Living Reviews in Solar Physics*, *6*, 3, doi:10.12942/lrsp-2009-3.

Dalmasse, K., G. Aulanier, P. Démoulin, B. Kliem, T. Török, and E. Pariat (2015), The Origin of Net Electric Currents in Solar Active Regions, *Astrophys. J.,* , *810*, 17, doi:10.1088/0004-637X/810/1/17.

Dalmasse, K., D. Nychka, S. Gibson, N. Flyer, and Y. Fan (2016), ROAM: a Radial-basis-function Optimization Approximation Method for diagnosing the three-dimensional coronal magnetic field, *Frontiers in Astronomy and Space Sciences*, *3*, 24, doi:10.3389/fspas.2016.00024.

de la Cruz Rodríguez, J., and H. Socas-Navarro (2011), Are solar chromospheric fibrils tracing the magnetic field?, *Astron. Astrophys.,* , *527*, L8, doi:10.1051/0004-6361/201016018.

De Rosa, M. L., C. J. Schrijver, G. Barnes, K. D. Leka, B. W. Lites, M. J. Aschwanden, T. Amari, A. Canou, J. M. McTiernan, S. Régnier, J. K. Thalmann, G. Valori, M. S. Wheatland, T. Wiegelmann, M. C. M. Cheung, P. A. Conlon, M. Fuhrmann, B. Inhester, and T. Tadesse (2009), A Critical Assessment of Nonlinear Force-Free Field Modeling of the Solar Corona for Active Region 10953, *Astrophys. J.,* , *696*, 1780–1791, doi:10.1088/0004-637X/696/2/1780.

del Toro Iniesta, J. C. (2003), *Introduction to Spectropolarimetry*, 244 pp.

del Toro Iniesta, J. C., and B. Ruiz Cobo (2016), Inversion of the radiative transfer equation for polarized light, *Living Reviews in Solar Physics*, *13*, 4, doi:10.1007/s41116-016-0005-2.

Demoulin, P., J. C. Henoux, E. R. Priest, and C. H. Mandrini (1996), Quasi-Separatrix layers in solar flares. I. Method., *Astron. Astrophys.,* , *308*, 643–655.

DeRosa, M. L., M. S. Wheatland, K. D. Leka, G. Barnes, T. Amari, A. Canou, S. A. Gilchrist, J. K. Thalmann, G. Valori, T. Wiegelmann, C. J. Schrijver, A. Malanushenko, X. Sun, and S. Régnier (2015), The Influence of Spatial resolution on Nonlinear Force-free Modeling, *Astrophys. J.,* , *811*, 107, doi:10.1088/0004-637X/811/2/107.

Dravins, D. (1974), Magnetic field and electric current structure in the chromosphere, *Solar Phys.*, *37*, 323–342, doi:10.1007/BF00152492.

Fan, Y. (2009), Magnetic Fields in the Solar Convection Zone, *Living Reviews in Solar Physics*, *6*, 4, doi:10.12942/lrsp-2009-4.

Fisher, G. H., D. W. Longcope, T. R. Metcalf, and A. A. Pevtsov (1998), Coronal Heating in Active Regions as a Function of Global Magnetic Variables, *Astrophys. J.,* , *508*, 885–898, doi:10.1086/306435.

Fisher, G. H., W. P. Abbett, D. J. Bercik, M. D. Kazachenko, B. J. Lynch, B. T. Welsch, J. T. Hoeksema, K. Hayashi, Y. Liu, A. A. Norton, A. S. Dalda, X. Sun, M. L. DeRosa, and M. C. M. Cheung (2015), The Coronal Global Evolutionary Model: Using HMI Vector Magnetogram and Doppler Data to Model the Buildup of Free Magnetic Energy in the Solar Corona, *Space Weather*, *13*, 369–373, doi:10.1002/2015SW001191.

Fleishman, G. D., and I. N. Toptygin (2013a), *712 p [FT13]*, *Cosmic Electrodynamics. Astrophysics and Space Science Library; Springer NY*, vol. 388.

Fleishman, G. D., and I. N. Toptygin (2013b), Stochastic particle acceleration by helical turbulence in solar flares, *Mon. Not. R. Astron. Soc.,* , *429*, 2515–2526, doi:10.1093/mnras/sts518.

Gary, D. E., G. D. Fleishman, and G. M. Nita (2013), Magnetography of Solar Flaring Loops with Microwave Imaging Spectropolarimetry, *Solar Phys.*, *288*, 549–565, doi:10.1007/s11207-013-0299-3.

Gary, G. A. (2001), Plasma Beta above a Solar Active Region: Rethinking the Paradigm, *Solar Phys.*, *203*, 71–86, doi:10.1023/A:1012722021820.

Gary, G. A., R. L. Moore, M. J. Hagyard, and B. M. Haisch (1987), Nonpotential features observed in the magnetic field of an active region, *Astrophys. J.,* , *314*, 782–794, doi:10.1086/165104.

Gelfreikh, G. B. (2004), Coronal Magnetic Field Measurements Through Bremsstrahlung Emission, in *Astrophysics and Space Science Library*, *Astrophysics and Space Science Library*, vol. 314, edited by D. E. Gary and C. U. Keller, p. 115, doi:10.1007/1-4020-2814-8-6.

Gibson, S., T. Kucera, S. White, J. Dove, Y. Fan, B. Forland, L. Rachmeler, C. Downs, and K. Reeves (2016), FORWARD: A toolset for multiwavelength coronal magnetometry, *Frontiers in Astronomy and Space Sciences*, *3*, 8, doi:10.3389/fspas.2016.00008.

Goodman, M. L. (2004), On the creation of the chromospheres of solar type stars, *Astron. Astrophys.,* , *424*, 691–712, doi:10.1051/0004-6361:20040310.

Gopasyuk, O. S. (2015), Rotation of sunspots in active region NOAA 10930, *Advances in Space Research*, *55*, 937–941, doi:10.1016/j.asr.2014.09.005.

Gosain, S., P. Démoulin, and M. López Fuentes (2014), Distribution of Electric Currents in Sunspots from Photosphere to Corona, *Astrophys. J.,* , *793*, 15, doi:10.1088/0004-637X/793/1/15.

Gudiksen, B. V., M. Carlsson, V. H. Hansteen, W. Hayek, J. Leenaarts, and J. Martínez-Sykora (2011), The stellar atmosphere simulation code Bifrost. Code description and validation, *Astron. Astrophys.,* , *531*, A154, doi:10.1051/0004-6361/201116520.

Gurevich, A. V. (1961), Behavior of Multiply Charged Ions in a Plasma, *Sov. Phys. JETP*, *13*, 1282–1286, doi:??

Hale, G. E., and S. B. Nicholson (1925), The Law of Sun-Spot Polarity, *Astrophys. J.,* , *62*, 270, doi:10.1086/142933.

Hansteen, V., N. Guerreiro, B. De Pontieu, and M. Carlsson (2015), Numerical Simulations of Coronal Heating through Footpoint Braiding, *Astrophys. J.,* , *811*, 106, doi:10.1088/0004-637X/811/2/106.

Harvey, J. W. (1969), Magnetic Fields Associated with Solar Active-Region Prominences., Ph.D. thesis, UNIVERSITY OF COLORADO AT BOULDER.

Hathaway, D. H. (2010), The Solar Cycle, *Living Reviews in Solar Physics*, *7*, 1, doi:10.12942/lrsp-2010-1.

Hénoux, J. C., and M. Karlický (2013), Flare line impact polarization. Na D2 589 nm line polarization in the 2001 June 15 flare, *Astron. Astrophys.,* , *556*, A95, doi:10.1051/0004-6361/201219478.

Hofmann, A., and J. Staude (1987), Electric current density in the sunspot photosphere derived from vector magnetograms, *Publications of the Astronomical Institute of the Czechoslovak Academy of Sciences*, *66*, 105–107.

Janvier, M., G. Aulanier, V. Bommier, B. Schmieder, P. Démoulin, and E. Pariat (2014), Electric Currents in Flare Ribbons: Observations and Three-dimensional Standard Model, *Astrophys. J.,* , *788*, 60, doi:10.1088/0004-637X/788/1/60.

Jiang, C., S. T. Wu, X. Feng, and Q. Hu (2016), Data-driven magnetohydrodynamic modelling of a flux-emerging active region leading to solar eruption, *Nature Communications*, *7*, 11522, doi:10.1038/ncomms11522.

Kazachenko, M. D., G. H. Fisher, B. T. Welsch, Y. Liu, and X. Sun (2015), Photospheric Electric Fields and Energy Fluxes in the Eruptive Active Region NOAA 11158, *Astrophys. J.,* , *811*, 16, doi:10.1088/0004-637X/811/1/16.

Keller, C. U., J. W. Harvey, and M. S. Giampapa (2003), SOLIS: an innovative suite of synoptic instruments, in *Innovative Telescopes and Instrumentation for Solar Astrophysics*, *Proc. SPIE*, vol. 4853, edited by S. L. Keil and S. V. Avakyan, pp. 194–204.

Kosugi, T., K. Matsuzaki, T. Sakao, T. Shimizu, Y. Sone, S. Tachikawa, T. Hashimoto, K. Minesugi, A. Ohnishi, T. Yamada, S. Tsuneta, H. Hara, K. Ichimoto, Y. Suematsu, M. Shimojo, T. Watanabe, S. Shimada, J. M. Davis, L. D. Hill, J. K. Owens, A. M. Title, J. L. Culhane, L. K. Harra, G. A. Doschek, and L. Golub (2007), The Hinode (Solar-B) Mission: An Overview, *Solar Phys.*, *243*, 3–17, doi:10.1007/s11207-007-9014-6.

Kotov, V. A. (1970), Magnetic field and electric currents of a unipolar sunspot., *Izvestiya Ordena Trudovogo Krasnogo Znameni Krymskoj Astrofizicheskoj Observatorii*, *41*, 67–88.

Kotov, V. A. (1971), On the Structure of Magnetic Field and Electric Currents of a Unipolar Sunspot (presented by a. Severny), in *Solar Magnetic Fields*, *IAU Symposium*, vol. 43, edited by R. Howard, pp. 212–219.

Kotov, V. A. (1972), Measurements of the Transverse Magnetic Field in the Chromosphere above a Sunspot., *Soviet Astron.*, *15*, 687–688.

Kramar, M., H. Lin, and S. Tomczyk (2016), Direct Observation of Solar Coronal Magnetic Fields by Vector Tomography of the Coronal Emission Line Polarizations, *Astrophys. J.,* , *819*, L36, doi:10.3847/2041-8205/819/2/L36.

Kusano, K., T. Maeshiro, T. Yokoyama, and T. Sakurai (2004), The Trigger Mechanism of Solar Flares in a Coronal Arcade with Reversed Magnetic Shear, *Astrophys. J.,* , *610*, 537–549, doi:10.1086/421547.

Lee, J. (2007), Radio Emissions from Solar Active Regions, *Space Science Rev.*, *133*, 73–102, doi:10.1007/s11214-007-9206-2.

Leka, K. D., R. C. Canfield, A. N. McClymont, and L. van Driel-Gesztelyi (1996), Evidence for Current-carrying Emerging Flux, *Astrophys. J.,* , *462*, 547, doi:10.1086/177171.

Levens, P. J., B. Schmieder, A. López Ariste, N. Labrosse, K. Dalmasse, and B. Gelly (2016), Magnetic Field in Atypical Prominence Structures: Bubble, Tornado, and Eruption, *Astrophys. J.,* , *826*, 164, doi:10.3847/0004-637X/826/2/164.

Lin, H., M. J. Penn, and S. Tomczyk (2000), A New Precise Measurement of the Coronal Magnetic Field Strength, *Astrophys. J.,* , *541*, L83–L86, doi:10.1086/312900.

Lites, B. W., V. Martinez Pillet, and A. Skumanich (1994), A quantitative comparison of vector magnetic field measurement and analysis techniques, *Solar Phys.*, *155*, 1–27, doi:10.1007/BF00670727.

Longcope, D. W., and B. T. Welsch (2000), A Model for the Emergence of a Twisted Magnetic Flux Tube, *Astrophys. J.,* , *545*, 1089–1100, doi:10.1086/317846.

Mackay, D. H., J. T. Karpen, J. L. Ballester, B. Schmieder, and G. Aulanier (2010), Physics of Solar Prominences: II. Magnetic Structure and Dynamics, *Space Science Rev.*, *151*, 333–399, doi:10.1007/s11214-010-9628-0.

Martínez Pillet, V., J. C. Del Toro Iniesta, A. Álvarez-Herrero, V. Domingo, J. A. Bonet, L. González Fernández, A. López Jiménez, C. Pastor, J. L. Gasent Blesa, P. Mellado, J. Piqueras, B. Aparicio, M. Balaguer, E. Ballesteros, T. Belenguer, L. R. Bellot Rubio, T. Berkefeld, M. Collados, W. Deutsch, A. Feller, F. Girela, B. Grauf, R. L. Heredero, M. Herranz, J. M. Jerónimo, H. Laguna, R. Meller, M. Menéndez, R. Morales, D. Orozco Suárez, G. Ramos, M. Reina, J. L. Ramos, P. Rodríguez, A. Sánchez, N. Uribe-Patarroyo, P. Barthol, A. Gandorfer, M. Knoelker, W. Schmidt, S. K. Solanki, and S. Vargas Domínguez (2011), The Imaging Magnetograph eXperiment (IMaX) for the Sunrise Balloon-Borne Solar Observatory, *Solar Phys.*, *268*, 57–102, doi:10.1007/s11207-010-9644-y.

Martínez-Sykora, J., B. De Pontieu, M. Carlsson, and V. Hansteen (2016), Misalignment between chromospheric features and magnetic field, *ArXiv e-prints*.

McClymont, A. N., and G. H. Fisher (1989), On the mechanical energy available to drive solar flares., *Washington DC American Geophysical Union Geophysical Monograph Series*, *54*, 219–225.

McClymont, A. N., L. Jiao, and Z. Mikic (1997), Problems and Progress in Computing Three-Dimensional Coronal Active Region Magnetic Fields from Boundary Data, *Solar Phys.*, *174*, 191–218, doi:10.1023/A:1004976720919.

Melrose, D. B. (1991), Neutralized and unneutralized current patterns in the solar corona, *Astrophys. J.,* , *381*, 306–312, doi:10.1086/170652.

Melrose, D. B. (1997), A Solar Flare Model Based on Magnetic Reconnection between Current-carrying Loops, *Astrophys. J.,* , *486*, 521–533.

Metcalf, T. R., L. Jiao, A. N. McClymont, R. C. Canfield, and H. Uitenbroek (1995), Is the solar chromospheric magnetic field force-free?, *Astrophys. J.,* , *439*, 474–481, doi:10.1086/175188.

Metcalf, T. R., K. D. Leka, G. Barnes, B. W. Lites, M. K. Georgoulis, A. A. Pevtsov, K. S. Balasubramaniam, G. A. Gary, J. Jing, J. Li, Y. Liu, H. N. Wang, V. Abramenko, V. Yurchyshyn, and Y.-J. Moon (2006), An Overview of Existing Algorithms for Resolving the 180 Ambiguity in Vector Magnetic Fields: Quantitative Tests with Synthetic Data, *Solar Phys.*, *237*, 267–296, doi:10.1007/s11207-006-0170-x.

Molodenskii, M. M. (1969), Integral Properties of Force-Free Fields., *Soviet Astron.*, *12*, 585.

Moreton, G. E., and A. B. Severny (1968), Magnetic Fields and Flares in the Region CMP 20 September 1963, *Solar Phys.*, *3*, 282–297, doi:10.1007/BF00155163.

Musset, S., N. Vilmer, and V. Bommier (2015), Hard X-ray emitting energetic electrons and photospheric electric currents, *Astron. Astrophys.,* , *580*, A106, doi:10.1051/0004-6361/201424378.

Nakariakov, V. M., and L. Ofman (2001), Determination of the coronal magnetic field by coronal loop oscillations, *Astron. Astrophys.,* , *372*, L53–L56, doi:10.1051/0004-6361:20010607.

Nita, G. M., G. D. Fleishman, A. A. Kuznetsov, E. P. Kontar, and D. E. Gary (2015), Three-dimensional Radio and X-Ray Modeling and Data Analysis Software: Revealing Flare Complexity, *Astrophys. J.,* , *799*, 236, doi:10.1088/0004-637X/799/2/236.

Orozco Suárez, D., A. Asensio Ramos, and J. Trujillo Bueno (2014), The magnetic field configuration of a solar prominence inferred from spectropolarimetric observations in the He i 10 830 Å triplet, *Astron. Astrophys.,* , *566*, A46, doi:10.1051/0004-6361/201322903.

Parenti, S. (2014), Solar Prominences: Observations, *Living Reviews in Solar Physics*, *11*, 1, doi:10.12942/lrsp-2014-1.

Parker, E. N. (1996), Inferring Mean Electric Currents in Unresolved Fibril Magnetic Fields, *Astrophys. J.,* , *471*, 485, doi:10.1086/177983.

Petrie, G. J. D. (2012), The Abrupt Changes in the Photospheric Magnetic and Lorentz Force Vectors during Six Major Neutral-line Flares, *Astrophys. J.,* , *759*, 50, doi:10.1088/0004-637X/759/1/50.

Pevtsov, A. A. (2005), Helicity Generation and Signature in Solar Atmosphere, *Highlights of Astronomy*, *13*, 89.

Pevtsov, A. A., and N. L. Peregud (1990), Electric currents in a unipolar sunspot, *Washington DC American Geophysical Union Geophysical Monograph Series*, *58*, 161–165, doi:10.1029/GM058p0161.

Pevtsov, A. A., R. C. Canfield, and T. R. Metcalf (1994), Patterns of helicity in solar active regions, *Astrophys. J.,* , *425*, L117–L119, doi:10.1086/187324.

Pevtsov, A. A., R. C. Canfield, and T. R. Metcalf (1995), Latitudinal variation of helicity of photospheric magnetic fields, *Astrophys. J.,* , *440*, L109–L112, doi:10.1086/187773.

Pevtsov, A. A., R. C. Canfield, and A. N. McClymont (1997), On the Subphotospheric Origin of Coronal Electric Currents, *Astrophys. J.,* , *481*, 973–977.

Pevtsov, A. A., V. M. Maleev, and D. W. Longcope (2003), Helicity Evolution in Emerging Active Regions, *Astrophys. J.,* , *593*, 1217–1225, doi:10.1086/376733.

Pevtsov, A. A., M. A. Berger, A. Nindos, A. A. Norton, and L. van Driel-Gesztelyi (2014), Magnetic Helicity, Tilt, and Twist, *Space Science Rev.*, *186*, 285–324, doi:10.1007/s11214-014-0082-2.

Puschmann, K. G., B. Ruiz Cobo, and V. Martínez Pillet (2010a), The Electrical Current Density Vector in the Inner Penumbra of a Sunspot, *Astrophys. J.,* , *721*, L58–L61, doi:10.1088/2041-8205/721/1/L58.

Puschmann, K. G., B. Ruiz Cobo, and V. Martínez Pillet (2010b), A Geometrical Height Scale for Sunspot Penumbrae, *Astrophys. J.,* , *720*, 1417–1431, doi:10.1088/0004-637X/720/2/1417.

Rachkovsky, D. N. (1962), Magnetic rotation effects in spectral lines, *Izvestiya Ordena Trudovogo Krasnogo Znameni Krymskoj Astrofizicheskoj Observatorii*, *28*, 259–270.

Rachkovsky, D. N. (1967), The reduction for anomalous dispersion in the theory of absorption line formation in a magnetic field, *Izvestiya Ordena Trudovogo Krasnogo Znameni Krymskoj Astrofizicheskoj Observatorii*, *37*, 56–61.

Raouafi, N.-E. (2002), Stokes parameters of resonance lines scattered by a moving, magnetic medium. Theory of the two-level atom, *Astron. Astrophys.,* , *386*, 721–731, doi:10.1051/0004-6361:20020113.

Raouafi, N. E., S. Patsourakos, E. Pariat, P. R. Young, A. C. Sterling, A. Savcheva, M. Shimojo, F. Moreno-Insertis, C. R. DeVore, V. Archontis, T. Török, H. Mason, W. Curdt, K. Meyer, K. Dalmasse, and Y. Matsui (2016), Solar Coronal Jets: Observations, Theory, and Modeling, *Space Science Rev.*, *201*, 1–53, doi:10.1007/s11214-016-0260-5.

Rayrole, J., and M. Semel (1970), Evaluation of the Electric Current in a Sunspot by the Study of the Observed Transverse Component of the Magnetic Field, *Astron. Astrophys.,* , *6*, 288–293.

Rudenko, G. V., and I. I. Myshyakov (2009), Analysis of Reconstruction Methods for Nonlinear Force-Free Fields, *Solar Phys.*, *257*, 287–304, doi:10.1007/s11207-009-9389-7.

Rust, D. M. (1994), Spawning and shedding helical magnetic fields in the solar atmosphere, *Geophys. Res. Lett.,* , *21*, 241–244, doi:10.1029/94GL00003.

Ryabov, B. I., V. P. Maksimov, S. V. Lesovoi, K. Shibasaki, A. Nindos, and A. Pevtsov (2005), Coronal Magnetography of Solar Active Region 8365 with the SSRT and NoRH Radio Heliographs, *Solar Phys.*, *226*, 223–237, doi:10.1007/s11207-005-2691-0.

Scherrer, P. H., J. Schou, R. I. Bush, A. G. Kosovichev, R. S. Bogart, J. T. Hoeksema, Y. Liu, T. L. Duvall, J. Zhao, A. M. Title, C. J. Schrijver, T. D. Tarbell, and S. Tomczyk (2012), The Helioseismic and Magnetic Imager (HMI) Investigation for the Solar Dynamics Observatory (SDO), *Solar Phys.*, *275*, 207–227, doi:10.1007/s11207-011-9834-2.

Schmieder, B., V. Archontis, and E. Pariat (2014), Magnetic Flux Emergence Along the Solar Cycle, *Space Science Rev.*, *186*, 227–250, doi:10.1007/s11214-014-0088-9.

Schou, J., P. H. Scherrer, R. I. Bush, R. Wachter, S. Couvidat, M. C. Rabello-Soares, R. S. Bogart, J. T. Hoeksema, Y. Liu, T. L. Duvall, D. J. Akin, B. A. Allard, J. W. Miles, R. Rairden, R. A. Shine, T. D. Tarbell, A. M. Title, C. J. Wolfson, D. F. Elmore, A. A. Norton, and S. Tomczyk (2012), Design and Ground Calibration of the Helioseismic and Magnetic Imager (HMI) Instrument on the Solar Dynamics Observatory (SDO), *Solar Phys.*, *275*, 229–259, doi:10.1007/s11207-011-9842-2.

Schrijver, C. J., M. L. De Rosa, T. R. Metcalf, Y. Liu, J. McTiernan, S. Régnier, G. Valori, M. S. Wheatland, and T. Wiegelmann (2006), Nonlinear Force-Free Modeling of Coronal Magnetic Fields Part I: A Quantitative Comparison of Methods, *Solar Phys.*, *235*, 161–190, doi:10.1007/s11207-006-0068-7.

Seehafer, N. (1990), Electric current helicity in the solar atmosphere, *Solar Phys.*, *125*, 219–232, doi:10.1007/BF00158402.

Semel, M., and A. Skumanich (1998), An ambiguity-free determination of J_Z in solar active regions, *Astron. Astrophys.,* , *331*, 383–391.

Severnyi, A. B. (1965), The Nature of Solar Magnetic Fields (The Fine Structure of the Field), *Soviet Astron.*, *9*, 171–182.

Shibata, K., and T. Magara (2011), Solar Flares: Magnetohydrodynamic Processes, *Living Reviews in Solar Physics*, *8*, 6, doi:10.12942/lrsp-2011-6.

Socas-Navarro, H. (2002), Zeeman diagnostics of solar magnetic fields, in *SOLMAG 2002. Proceedings of the Magnetic Coupling of the Solar Atmosphere Euroconference*, *ESA Special Publication*, vol. 505, edited by H. Sawaya-Lacoste, pp. 45–51.

Socas-Navarro, H. (2005a), The Three-dimensional Structure of a Sunspot Magnetic Field, *Astrophys. J.,* , *631*, L167–L170, doi:10.1086/497334.

Socas-Navarro, H. (2005b), Are Electric Currents Heating the Magnetic Chromosphere?, *Astrophys. J.,* , *633*, L57–L60, doi:10.1086/498145.

Solanki, S. K., A. Lagg, J. Woch, N. Krupp, and M. Collados (2003), Three-dimensional magnetic field topology in a region of solar coronal heating, *Nature*, *425*, 692–695, doi:10.1038/nature02035.

Tomczyk, S., G. L. Card, T. Darnell, D. F. Elmore, R. Lull, P. G. Nelson, K. V. Streander, J. Burkepile, R. Casini, and P. G. Judge (2008), An Instrument to Measure Coronal Emission Line Polarization, *Solar Phys.*, *247*, 411–428, doi:10.1007/s11207-007-9103-6.

Unno, W. (1956), Line Formation of a Normal Zeeman Triplet, *PASJ*, *8*, 108.

Valori, G., B. Kliem, and M. Fuhrmann (2007), Magnetofrictional Extrapolations of Low and Lou's Force-Free Equilibria, *Solar Phys.*, *245*, 263–285, doi:10.1007/s11207-007-9046-y.

Wang, Z., D. E. Gary, G. D. Fleishman, and S. M. White (2015), Coronal Magnetography of a Simulated Solar Active Region from Microwave Imaging Spectropolarimetry, *Astrophys. J.,* , *805*, 93, doi:10.1088/0004-637X/805/2/93.

Warren, H. P. (2014), Measurements of Absolute Abundances in Solar Flares, *Astrophys. J.,* , *786*, L2, doi:10.1088/2041-8205/786/1/L2.

Wheatland, M. S. (2000), Are Electric Currents in Solar Active Regions Neutralized?, *Astrophys. J.,* , *532*, 616–621, doi:10.1086/308577.

Wheatland, M. S. (2007), Calculating and Testing Nonlinear Force-Free Fields, *Solar Phys.*, *245*, 251–262, doi:10.1007/s11207-007-9054-y.

Wheatland, M. S., P. A. Sturrock, and G. Roumeliotis (2000), An Optimization Approach to Reconstructing Force-free Fields, *Astrophys. J.,* , *540*, 1150–1155, doi:10.1086/309355.

White, S. M. (2005), Radio Measurements of Coronal Magnetic Fields, in *Chromospheric and Coronal Magnetic Fields*, *ESA Special Publication*, vol. 596, edited by D. E. Innes, A. Lagg, and S. A. Solanki, p. 10.1.

Wiegelmann, T., and B. Inhester (2010), How to deal with measurement errors and lacking data in nonlinear force-free coronal magnetic field modelling?, *Astron. Astrophys.,* , *516*, A107, doi:10.1051/0004-6361/201014391.

Wiegelmann, T., and T. Sakurai (2012), Solar Force-free Magnetic Fields, *Living Reviews in Solar Physics*, *9*, 5, doi:10.12942/lrsp-2012-5.

Wiegelmann, T., B. Inhester, and T. Sakurai (2006), Preprocessing of Vector Magnetograph Data for a Nonlinear Force-Free Magnetic Field Reconstruction, *Solar Phys.*, *233*, 215–232, doi:10.1007/s11207-006-2092-z.

Wiegelmann, T., J. K. Thalmann, C. J. Schrijver, M. L. De Rosa, and T. R. Metcalf (2008), Can We Improve the Preprocessing of Photospheric Vector Magnetograms by the Inclusion of Chromospheric Observations?, *Solar Phys.*, *247*, 249–267, doi:10.1007/s11207-008-9130-y.

Wiegelmann, T., J. K. Thalmann, and S. K. Solanki (2014), The magnetic field in the solar atmosphere, *A&A Rev.*, *22*, 78, doi:10.1007/s00159-014-0078-7.

Zhang, H., and S. Bao (1998), Latitudinal distribution of photospheric current helicity and solar activities, *Astron. Astrophys.,* , *339*, 880–886.

Corresponding author: Gregory D. Fleishman, Physics Department, Center for Solar-Terrestrial Research, New Jersey Institute of Technology Newark, NJ, 07102-1982, USA. (gfleishm@njit.edu)